Doctoral Dissertation

Efficient Error Correction Solutions for Flicker Free Visible Light Communication Systems

Dinh-Dung Le

August 15, 2019

Graduate School of Information Science
Nara Institute of Science and Technology

A Doctoral Dissertation
submitted to Graduate School of Information Science,
Nara Institute of Science and Technology
in partial fulfillment of the requirements for the degree of
Doctor of ENGINEERING

Dinh-Dung Le

Thesis Committee:

Professor Yasuhiko Nakashima	(Supervisor)
Professor Minoru Okada	(Co-supervisor)
Associate Professor Takashi Nakada	(Co-supervisor)
Assistant Professor Thi-Hong Tran	(Co-supervisor)
Assistant Professor Renyuan Zhang	(Co-supervisor)

Efficient Error Correction Solutions for Flicker Free Visible Light Communication Systems*

Dinh-Dung Le

Abstract

In this thesis, we research about the visible light communication (VLC) system, in which forward error correction (FEC) and run-length limited (RLL) codes are implemented to ensure reliable data transmission and mitigate flicker, respectively. Several combinations of RLL and FEC codes have proposed in the literature. However, these solutions are not able to achieve high error-correction performance because typical RLL codes only support hard decoding schemes.

In the first part of this study, we propose the use of RLL code in serial concatenation with the Polar code as an FEC for VLC. To improve error-correction capability, we employ the soft-input soft-output RLL decoding scheme which produces soft-information for Polar decoder afterward. This soft RLL-Polar decoding scheme obtains best bit error rate (BER) compared with previous works.

Improving the reliability with soft RLL-Polar decoder requires accurate knowledge of the VLC channel, which is challenging to acquire in practical VLC system. The second part of this study proposes a low-bit demodulator to calculate soft-input for RLL-FEC decoding scheme. This demodulator makes use low-bit analog to digital converter (ADC) to determine the confidence bits of the received signal and statistically characterize the VLC channel to generate soft information to be provided to the soft RLL-FEC decoder.

To reduce complexity, which is the main drawback of soft RLL-FEC decoding scheme, we propose deep learning based decoders which replace the concatenation of RLL and FEC decoder in the last part of this thesis. The proposed

*Doctoral Dissertation, Graduate School of Information Science, Nara Institute of Science and Technology, August 15, 2019.

approach consists of a one-layer recurrent neural network (RNN) followed by a fully-connected layer. We also propose the use of low-bit demodulator to generate the input data for the RNN structure. The numerical results show that the proposed RNN-based decoders for short block lengths are capable of achieving close error-correction performance to the state-of-the-art decoder while the processing speed is improved significantly.

Keywords:

Forward Error Correction (FEC), Visible Light Communication (VLC), Flicker Mitigation, Run Length Limited (RLL), Deep Learning (DL)

List of publications

Journal (J)

J1. Dinh-Dung Le, Duc-Phuc Nguyen, Thi-Hong Tran, Yasuhiko Nakashima, "A Deep Learning-based Joint RLL-FEC Decoding Scheme for Visible Light Communication," submitted to *EURASIP Journal on Wireless Communications and Networking* (Under review). [Corresponds to Chapter 5]

J2. Dinh-Dung Le, Duc-Phuc Nguyen, Thi-Hong Tran, Yasuhiko Nakashima, "Log-Likelihood Ratio Calculation using 3-bit Soft-Decision for Error Correction in Visible Light Communication Systems," in *IEICE Transactions on Fundamentals*, vol.E101-A, no.12, pp.2210-2212, Dec. 2018. [Corresponds to Chapter 4]

J3. Dinh-Dung Le, Duc-Phuc Nguyen, Thi-Hong Tran, Yasuhiko Nakashima, "Joint Polar and Run-Length Limited Decoding Scheme for Visible Light Communication" in *IEICE Communication Express*, vol.7, issue 1, pp.19-24, Jan. 2018. [Corresponds to Chapter 3]

International Conferences (I) (Peer Review)

I1. Duc-Phuc Nguyen, Dinh-Dung Le, Thi-Hong Tran, Huu-Thuan Huynh, Yasuhiko Nakashima, "Hardware Implementation of A Non-RLL Soft-decoding Beacon-based Visible Light Communication Receiver," in *IEEE International Conference on Advanced Technologies for Communications (ATC'18)*, pp.195-200, October 2018.

I2. Duc-Phuc Nguyen, Dinh-Dung Le, Thi-Hong Tran, Yasuhiko Nakashima, "Non-RLL DC-Balance based on a Pre-scrambled Polar Encoder for Beacon-based Visible Light Communication Systems," in *International Conference and Exhibition on Visible Light Communication 2018 (ICEVLC2018)*, pp.1-4, Yokohama, Japan, March 16, 2018.

I3. Duc-Phuc Nguyen, Dinh-Dung Le, Dai Long Hoang, Satoya Yoshida, Thi-Hong Tran, Yasuhiko Nakashima, "A Beacon-based Visible Light Communi-

cation System applied in Precise Indoor Localization for Smart Shopping," in *International Conference for Top and Emerging Computer Scientist 2017 (IC-TECS 2017)*, Taipei, Taiwan, December 2017. (Dinh-Dung Le made presentation and won 1'st prize in poster presentation).

Domestic Conferences (D) (Non Peer Review)

D1. Dinh-Dung Le, Duc-Phuc Nguyen, Thi-Hong Tran, Yasuhiko Nakashima, Son-Kiet Nguyen, Huu-Thuan Huynh, "A Prototype of Dimmable Visible Light Communication System on FPGA" in *IEICE Technical Committee on Computer Systems (CPSY) HotSPA2017*, Vol. 117, Issue 45, pp.9-13, Hokkaido, Japan, May 22-24, 2017.

Contents

List of Figures

List of Tables

1 Introduction

This part firstly discusses the research motivation of VLC systems. Next, the overview of the problem what this dissertation addressed is presented. Then, the research contribution, scope and limitation are included. Finally, the rest of this part shows the dissertation layout.

1.1 Research Motivation

Internet of Things (IoT), which connects various things to each other and the Internet, is one of most important technology around the world today. It is expected that by the year 2022, 28.5 billion networked devices will be connected to the Internet and IoT devices will occupied more than half of the total connected devices [3]. At the same time, wireless and mobile devices are projected account for apprioximately 71% of total Internet traffic. It is clear that wireless communication is the basic platform for the development of IoT technology.

The increasing number of wireless devices and data traffic have strong impact on the wireless spectrum in term of contention, interference, and increased noise floor. Consequenly, the current used wireless spectrum might not be sufficent to sastisfy the demand of mobile users in future. A promising solution for this problem is developing new wireless communication technologies in other radio-frequency bands. For instance, Low Power Wide Area Network (LoRaWAN), Sigfox, IEEE 802.11ah, and Wi-SUN are new wireless standards targeted for low power IoT applications using the Sub-Gigahertz frequency bands [4]. Between 30 and 300 GHz, milimeter-wave (mmWave) communications have received great attentions [5]. In the optical spectrum regions, optical wireless communication (OWC) technology based on infrared, visible light, and laser wavelenghs are also taken into account.

In recent years, ilumination technology has experienced enormous changes due to the revolution of light-emitting diodes (LEDs). The LED lighting has outstanding advantages when compared with the conventional lighting sources [6]. With the creation of white light, the lamps using LEDs can provide higher efficiency in lumen output while the power consumption is the same or lower. Because of the flexible in size and arrangement possibilities, LED can be use in

convetional lighting and easily intergrated with different kind of products. Combining with dimming, change of colours and other control options, the lighting system can sastify the aesthetics requirements and various environments. Moreover, the LED bulbs are generally have longer life and lower cost due to the inceasing in lighting market and the development of manufactoring. As a result, there is a significant transformation in lighting system from using conventional light sources to using LEDs. Japan Lighting Manufactures Association (JLMA) has forecasted that 50% of existing luminaires on the market is Solid State Lighting (SSL) luminaires in 2020 and this ratio will be 100% by the year 2030 [7]. Assuming that the number of existing luminaires on the market in 2020 and 2030 will remain unchanged from 2006, JLMA also predicted that the power consumption for lighting purpose will be reduced nearly 30% and 48% from 1649 hundred million kWh in 2006 to 1162 hundred million kWh and 863 hundred million kWh in 2020 and 2030, respectively.

The development of new wireless communication technology and the popular of LEDs in lighting systems are the motivation for researches about Visible Light Communication, which is also the main target of the works in this dissertation.

1.2 Overview of the Problem

In wireless communication systems, it is very necessary to develop new technologies that will guarantee the transmission over the wireless channel. For the visible light communication systems, this requirement becomes more significant since the light are often limited by several forms of noises and interferences from various sources. That is why, Forward Error Correction (FEC) codes are essential to ensure a reliable data transmission and consiquently extend the distances. Since hard-decision FEC schemes are widely used in these VLC systems because receivers are only capable of recognizing logical values 0 and 1, they are inferior to soft-decision FEC codes in terms of decoding performance. This research will focus on applying soft-decision FEC codes in VLC systems.

Another main challenge for communication using visible light spectrum is flicker mitigation [8]. Flicker refers to the fluctuation of the light's intensity resulting from modulating information into light sources. Since illumiating is the primary purpose in VLC systems, any flicker which could be cause of adverse

effects on human physilogy must be mitigated. Flickering can be avoided when the fuctuation in LED's intensity must be smaller than the maximum flicker period (MFTP) which is defined as the maximum time period over which the light brightness can change without human eye perceiving it [9]. In general, a frequency greater than 200Hz or MFTP $<$ 5ms is considered safe for human eyes [10].

1.3 Research Contribution

The first contribution of this dissertation is the use of RLL and Polar codes which is related to publication (J3). In this research, we implement the soft-input soft-output (SISO) RLL decoder to produce the log-likelihood ratios (LLRs) for Polar decoder. This combination of SISO RLL-Polar decoding scheme improves the error-correction performance of VLC system, but requires more computational cost of the decoding process.

The other contribution is the method to calculate the LLRs for practical VLC system which is related to publication (J2). When the LED's light strikes the photodetector, a voltage is generated in the external circuit proportional to the intensity of the incident light. To calculate the soft information, the researcher proposes a low-bit demodulator to quantize the received voltage into binary sequences. In addition, we statistically characterize the VLC channel to generate soft information to be provided to the soft RLL-FEC decoder.

The third contribution is the deep learning (DL) based decoders which replace the concatenation of RLL and FEC decoder. The proposed joint RLL-FEC decoding method combines low-bit ADCs and light-weight recurrent neural networks (RNNs) architecture. We confirm that DL-based decoder can recover the original data at VLC receiver with slight error-correction performance loss and significantly improving in the computation complexity compared to the state-of-the-art decoder. The computation time of the proposed decoders on various hardware platforms confirms the capability of using DL-based decoders with flicker mitigation in VLC system.

1.4 Scope and Limitation

The scope of this research includes the theorical designs of the RLL-FEC decoders in VLC system. The first task includes the formulation of the signal model of the receiver, the design of low-bit demodulation, and the architecture of DL-based decoder. The second task is the implementation of the model using simulations. The simulation results include the BER performance of the proposed systems. This dissertation does not cover real experiments and hardware implementation of the decoder; hence, those can be considered as the limitations of this study.

1.5 Dissertation Layout

The dissertation is divided into six chapters. Chapter 1 presents the introduction that includes the motivation, overview ò the problem, contributions and limitation of this research. Chapter 2 discusses the overview and system model of VLC. The related works of this research is also introduced in the last part of Chapter 2. Chapter 3 presents the concaternation of SISO RLL and Polar decoding schemes in VLC system. Chapter 4 contains the detailed discussion about log-likelihood ratio calculation method for practical VLC system. Chapter 5 presents the proposed joint RLL-FEC decoder using deep learning approach. Finally, the last chapter concludes the dissertation.

2 Background

In this chapter, an overview of the Visible Light Communication systems and its applications, which are the main target of the work presented in this dissertation, is firstly presented in Section 2.1. Then, a brief decription of Forward Error Control, Polar Code, and Runlength Limited Code are presented

2.1 Overview of Visible Light Communication and its applications

Visible Light Communication (VLC) as a subfield of optical wirless communication (OWC) provides data transmission as an additional functionality to illumination systems. Due to the increasing difficuities of current RF technologies and the huge growth of LEDs devices, VLC has recently attracted increasing attention from academia and industry. This technology, which uses the visible light spectrum in the wavelength interval of 380 - 720 nm as communication medium, offers several interesting advantages over conventional wireless communication technologies:

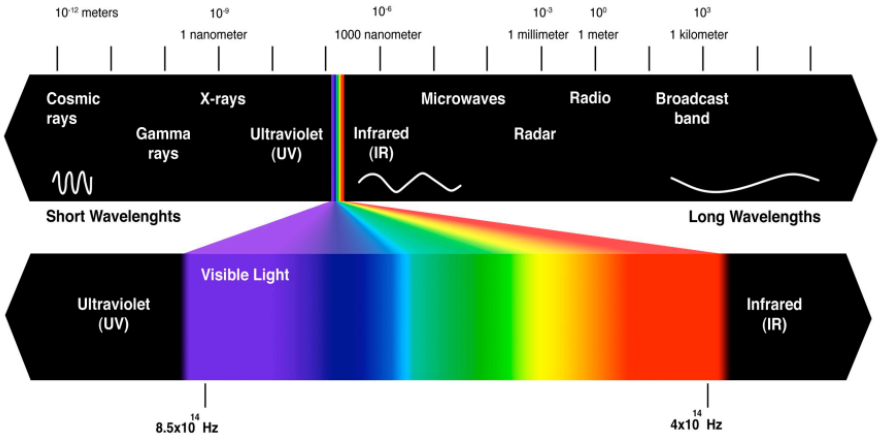

Figure 2.1. Electromagnetic spectrum usage [1].

- Large frequency spectrum bandwidth with more than 300THz.
- Free licensed spectrum and available for immediate installasion.

- Secure data communication.
- Low power consumption and low cost technology.
- Zero electromagnetic interference (EMI).
- Human friendly communication system.

From the first efforts of using LEDs for both illumination and data communication proposed by researchers in Keio University (Japan) in 2000 [11], futher intensitive research was being investigated in VLC domain worldwide. In November 2003, with aiming to publicize and standardize the VLC technology, the Visible Light Communication Consortium (VLCC) was established. By 2007, the VLCC introduced two VLC standards including Visible Light Communication System and Visible Light ID System which were aterwards approved by Japan Electronics and Information Technology Industries Association (JEITA) JEITA CP-1221 and CP-1222, respectively. In 2011, the Institute of Electrical and Electronics Engineers (IEEE) proposed the IEEE 802.15.7 standard for short-range WOC using VLC with flicker mitigation and dimming support.

2.2 VLC applications

By taking benefits of the mentioned advantages, the VLC technology can be applied in numerous application domains. In general, the VLC applications can be used as a complementary solution for the current wireless technology to improve the overall performance. The most presentative VLC applications are summaried hereafter.

Light Fidelity (Li-Fi)

Li-Fi, which was first coined by professor Harald Haas in 2011 [12], makes use the huge available bandwidth of VLC technology to achive high speed, secure, bidirectional, and fully networked wireless communications [13]. By 2016, complete cellular networks based on Li-Fi with peak transmission speeds of 8 Gbps from a single LED have been introduced. The development of Li-Fi has led to the formation of the IEEE 802.11bb task group which will response for the global Li-Fi standard in 2017.

Intelligent Transportation System (ITS)

Along with the replacement of conventional illumination in traffic lights and vehicles lighting systems by LEDs, the possibility to use VLC to interact between infrastructure and vehicles (I2V), as well as between vehicles (V2V), has become an active research topic for ITS applications [2, 14, 15]. The application of VLC technology in ITS is illustrated in Figure 2.2. In the case of I2V-VLC, traffic light systems broadcast the information which are received by the vehicles in the road. In the case of V2V-VLC, the vehicles use the rear and front LED which originally for signalling to exchange the messages.

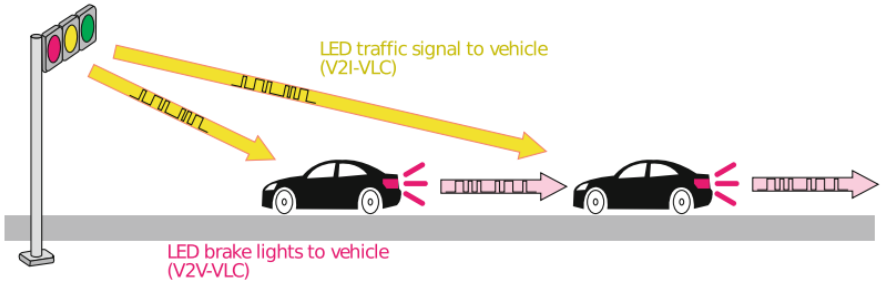

Figure 2.2. The main use cases of technology in ITS [2].

Indoor Positioning System

In the field of positioning, VLC based systems use LEDs to transmit the position signals which may contain the ID or the location of the LEDs, while the PDs or image sensors are used for receiving it [16, 17, 18]. These systems could be also used to create smart places by providing geo-localized information. For examples, the informations about the exhibits can be sent to user devices by using the indoor light in the museums [19].

LED to Camera Communication

Recently, image sensors integrated in smart devices, especially the Complemnetary Metal-Oxide-Semiconductor (CMOS) sensors, have become more and more popular. As a result, the LED to Camera Communication system is attractive among various VLC research and applications. The rolling shutter affect of the CMOS sensor is used to increase the data transmission rate and build ITS systems [20, 21], as well as a low cost and reliable bi-directional VLC system for IoT applications [22].

Underwater Wireless Communication

Underwarter communication is always attractive great interest of the military, industry, and scientific community. However, current underwater communication applications using wire link are usually restricted by their hight installation cost, operational difficultied and lack of flexibility [23]. While wireless communication is a promising alternative to overcome these limitations, underwater visible light communication has emerged as cost effective, enery efficent and hight data rate compared with communication using RF and acoustic waves [24].

2.3 VLC system model

In VLC systems, LED is used to emit the optical signal at the transmitter. After passing through the VLC channel, the receiver collects the transmitted signal using a photoditector. Other light signals (known as optical noises), which affect the VLC communication quality, are also received. Figure 2.3 shows a basic block diagram of a VLC system.

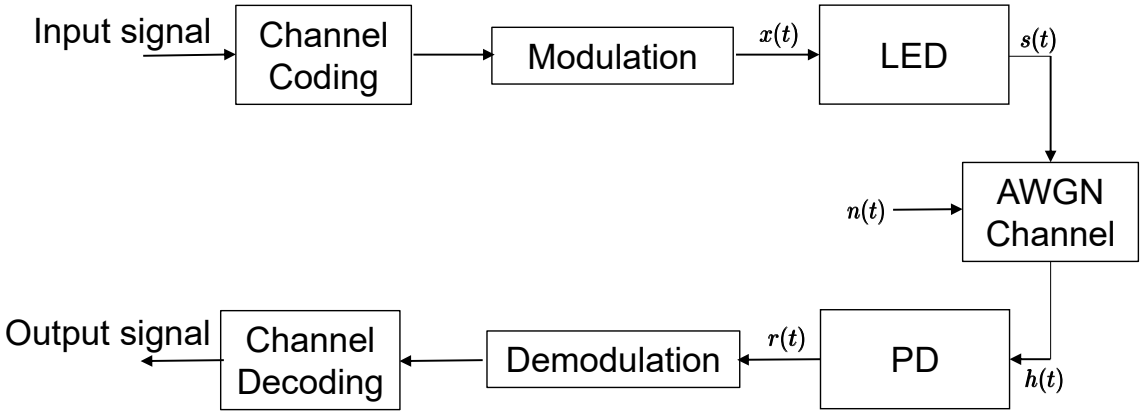

Figure 2.3. Block diagram of a typical VLC system.

In general, the VLC channel is related closely to three main parameters which are the opical signal from LED, impulse response, and received signal at PD. The VLC systems are highly sensitive to the direct expose of the PD to any high power visible light sources. The ambient light striking the PD are mainly at direct current (DC) and can be filtered out by using optical band pass filter. However, they leads to a steady shot noise that can be considered as a Gaussian

noise process [25]. Consequently, the VLC channle can be modeled as an Additive White Gaussian Noise (AWGN) channel [26] as the following:

$$y(t) = \gamma x(t) * h(t) + n(t) \tag{2.1}$$

Here, the PD current $y(t)$ is a result of the convolution between the power of emitted signal $x(t)$ and the impulse response $h(t)$; $*$ denotes convolution; γ is the detector responsivity (A/W); and $n(t)$ is Additive White Gaussian Noise $(AWGN)$. Considering the geometry in Figure 2.3, the DC gain $H(0)$ of a LOS VLC channel is expressed by [27]

$$H(0) = \begin{cases} \dfrac{(m+1)A}{2\pi d^2}\cos^m(\varphi)T_s(\theta)g(\theta)\cos(\theta), & 0 \leq \theta \leq \Psi_c \\ 0, & \theta > \Psi_c \end{cases} \tag{2.2}$$

where A is the phyiscal area of PD and T_s is the filter transmission coefficent. Ψ_c is the PD's fiew of view (FOV) and d is the distance between a transmitter and a receiver. θ is the incidence angle of the radiation and m is the lampertian emission index, which is a key parameter specifying the directivity of the transmitters [28].

In general, the half-power angle $\Phi_{1/2}$, which is the angle between emitting direction and the axis, has a remarkable influence on the coverage range and pattern shape of the lambertian light source. It is used to calculate the ampertian emission index as the following:

$$m = \frac{-\ln 2}{\ln(\cos_{\Phi_{1/2}})}, \tag{2.3}$$

Moreover, the gain of an optical concentrator can be calculated by

$$g(\theta) = \begin{cases} \dfrac{n^2}{\sin^2 \Psi_c}, & 0 \leq \theta \leq \Psi_c \\ 0, & \theta > \Psi_c \end{cases} \tag{2.4}$$

where n represents the internal reflective index of the optical concentrator used in the receiver side. Consequently, the average power of received signal P_r is calculated as

$$P_r = P_t + H(0), \tag{2.5}$$

where $P_t = \frac{1}{T}\int_0^T x(t)d()t$ is the average power of transmitted signal; T denotes the light signal duration.

In addition, total noise variance N of the VLC channel, which is the sum of shot and thermal noise [26], yields in

$$N = \sigma_{shot}^2 + \sigma_{thermal}^2, \tag{2.6}$$

A variance of shot noise is given as

$$\sigma_{shot}^2 = 2q\gamma P_r B + 2q\gamma I_{bg} I_2 B, \tag{2.7}$$

where q is the electronic charge, B is equivalent noise bandwidth, I_{bg} is the background current, and I_2 is the noise bandwidth factor which is denifed as $I_2 = 0.562$.

Assuming that a p-i-n/FET transimpedance receiver is used in this model, the thermal noise variance is the sum of feedback-resistor noise and FET channel noise, given as

$$\sigma_{thermal}^2 = \frac{8\pi k T_K}{G}\eta A I_2 B^2 \ + \ \frac{16\pi^2 k T_K \Gamma}{g_m}\eta^2 A^2 I_3 B^3, \tag{2.8}$$

where k is the Boltzmann's constant, T_K is the absolute temperature, G is the open-loop voltage gain, η is the fixed capacitance of photo detector per unit area, Γ is the FET channel noise factor, g_m is the FET transconductance, and $I_3 = 0.0868$. Finally, the received signal-noise-ratio (SNR_{rx}) is expressed by

$$SNR_{rx} = \frac{S}{N} \ = \ \frac{\gamma^2 P_r^2}{\sigma_{shot}^2 + \sigma_{thermal}^2} \tag{2.9}$$

2.4 Related Works

In on-off keying intensity modulation with direct detection (OOK IM/DD) VLC systems, the information is typically conveyed via an LED in the forms of optical power. As a result, the long runs of 1's and 0's in the data may cause perceived fluctuation in light intensity, also known as flicker, which may have detrimental effects on the user's experience. Run-length limited (RLL) codes are widely used to avoid flicker because of its simplicity. In fact, by breaking the random input

Table 1. VLC channel Parameters.

T_s	Filter transmission coeficient
γ	PD responsivity
A	Phyiscal area of PD
Ψ_c	Receiver's Field of View
d	Distance between LED and PD
θ	Incidence angle of the radiation
m	Lampertian emission index
$\Phi_{1/2}$	Half-power angle
n	Internal reflective index
q	Electronic charge
B	Noise bandwidth
I_{bg}	Background noise current
I_2	Noise bandwidth factor
k	Boltzmann's constant
T_K	Absolute temperature
G	Open-loop voltage gain
η	Fixed capacitance of PD
Γ	FET channel noise factor
g_m	FET transconductance
I_3	Noise bandwisth factor for a full raised-cosine pulse shape

data into codewords which have an equal number of 1's and 0's (DC balance), RLL codes help maintain a stable brightness which is also an essential requirement to support dimming control for illumination purpose. Moreover, forward error control (FEC) codes are also applied to enable reliable communication over VLC channels.

According to IEEE 802.15.7 standard [29], three well-known RLL codes including Manchester, 4B6B code, and 8B10B code are employed to incorporate FEC codes such as Reed-Solomon (RS) codes or the concatenation between RS codes and convolutional code (CC). RLL codes generally show a weak error control ability, produce more coding overheads, and only work with hard decoding. These drawbacks significantly limit the error correction performance of FEC

codes. Therefore, a considerable number of studies have been conducted on improving the coding gain and mitigating flicker in VLC systems.

On top of that, two FEC schemes based on modified Reed-Muller (RM) codes have been proposed for OOK-based VLC systems [30, 31]. Although these methods can guarantee DC balance at precisely 50%, their error control performances are inferior compared with turbo codes, low-density parity-check (LDPC) codes, and polar codes. In the turbo code-based scheme proposed by Lee and Kwon [32], an acceptable number of 1's and 0's at the output are created by puncturing and pseudo-noise sequence scrambling techniques [32]. Also, an adaptive FEC scheme based on LDPC code is introduced for dimmable VLC systems [33]. This proposal can achieve good bit-error-rate (BER) performance; however, the fixed code rate 1/2 LDPC code, puncturing technique, and Manchester code are employed for DC balance. Another coding scheme based on the fountain code and scrambler, which has dramatically improved the transmission efficiency, is mentioned in [34]. However, this scheme requires feedback information which is not suitable in OOK-based VLC systems.

A non-RLL polar-code-based solution has recently proposed for dimmable VLC systems [35]. This approach has shown promising results in weight distribution and run-length distribution. The biggest obstacle of this proposal is the equal probabilities of short runs of 1's and 0's can only be achieved with a long codeword; as chosen to be 2048. Zunaira *et al.* have proposed replacing the conventional RLL codes with a recursive Unity-Rate Code (URC) or an Unary-Code as the inner code, and a 17-subcode IRregular Convolutional Code (IRCC) is selected for the outer code [36]. Although these methods can achieve different dimming levels with good BER performance; however, the system latency increase due to iterative-decoding schemes.

To overcome the limitation of conventional RLL codes, new RLL (soft-RLL) codes were also proposed for VLC systems [37, 38, 39]. Soft-RLL codes permit soft-decoding of FEC algorithms to be applied to improve the BER performance. Since the VLC systems use direct detection method at receiver, calculating the probabilities of received codewords or the log-likelihood ratios (LLRs) is also a hard problem. Moreover, hardware implementation is unfeasible because it requires massive computational efforts, with many additions and multiplications.

Recently, Le *et al.* have proposed a LLRs calculation method for VLC system [40].

3 Joint RLL-Polar Decoding Scheme for Visible Light Communication Systems

3.1 Proposed System

In this section, we primarily focus on the downlink transmission of VLC systems. The block diagram of system is shown in Figure. 3.1. Assuming n-bit codeword c is generated after passing information vector u with k bit length through Polar FEC encoder block. Then, the LUT-based (q, s) RLL encoder block is used to map every q-bit groups in c to s-bit groups in $\bar{c}$, based on the mapping rule M that guarantees the DC balance in the system. Finally, $\bar{c}$ is converted into OOK signal $x(t)$ and emitted through the channel $h(t)$ by Light Emitted Diode (LED) front-end circuit.

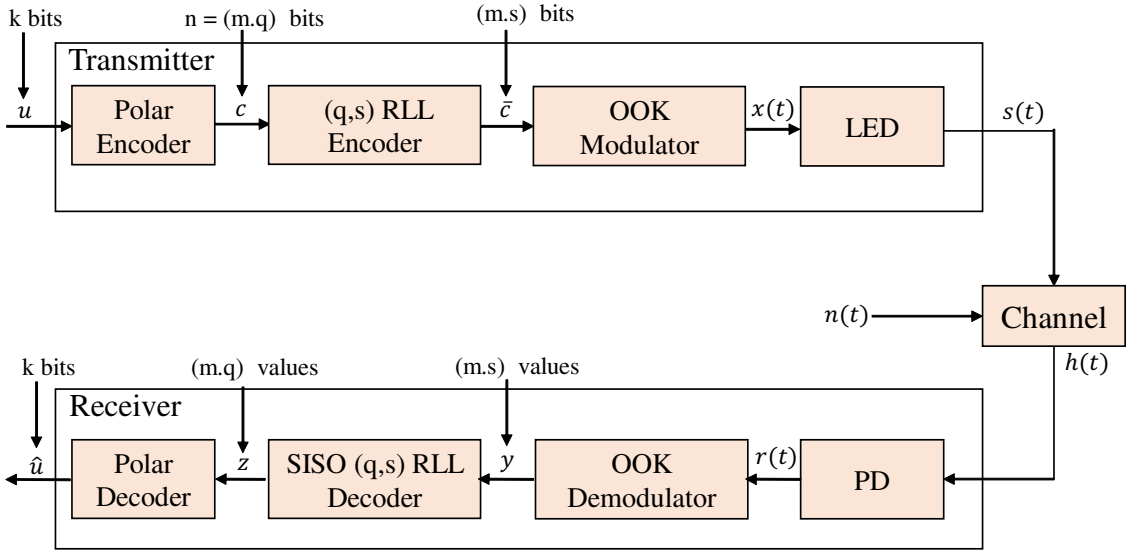

Figure 3.1. Block diagram of the proposed VLC system.

The photodiode (PD) receives the signal $r(t) = R.s(t) * h(t) + n(t)$, where R is the receiver responsivity (A/W); $*$ denotes convolution; and $n(t)$ is Additive White Gaussian Noise $(AWGN)$ which contains shot and thermal noises with the variance σ^2 [26]. Using match filter at the output of OOK demodulator, photo

current values y for the Soft-Input Soft-Output $SISO$ (q, s) RLL decoder are generated. From s values y_i in y, the SISO calculates 4 new Log-Likelihood Ratio (LLR) values z_i for Polar decoder to estimates the transmitted information $\hat{u}$.

3.2 Soft Input Soft Ouput Runlengh Limited Codes

The (q, s) RLL encoder of Figure 3.1 takes the $(m.q)$-bits codeword of Polar encoder as its input $c = [c_1, c_2, ..., c_i, ..., c_m]$, where $c_i = [c_i^{(1)}, c_i^{(2)}, ..., c_i^{(q)}]$, to create $(m.s)$-bits output $\bar{c} = [\bar{c}_1, \bar{c}_2, ..., \bar{c}_i, ..., \bar{c}_m]$, where $\bar{c}_i = [\bar{c}_i^{(1)}, \bar{c}_i^{(2)}, ..., \bar{c}_i^{(s)}]$.
In the receiver, the inputs of RLL decoder are soft values that defined as $y = [y_1, y_2, ..., y_i, ..., y_m]$, where $y_i = [y_i^{(1)}, y_i^{(2)}, ..., y_i^{(s)}]$; similarly, the outputs of the RLL decoder are represented as $z = [z_1, z_2, ..., z_i, ..., z_m]$, where $z_i = [z_i^{(1)}, z_i^{(2)}, ..., z_i^{(q)}]$.
Based on this notation, the decoding algorithm is summarized as follow:

1. Each bit probabilities of '0' and '1' based on OOK in AWGN channel can be calculated as

$$p(y_i^{(j)}|\bar{c}_i^{(j)} = 0) = \frac{1}{\sqrt{2\pi\sigma^2}} e^{-\frac{y_i^{(j)}}{2\sigma^2}} \tag{3.1}$$

$$p(y_i^{(j)}|\bar{c}_i^{(j)} = 1) = \frac{1}{\sqrt{2\pi\sigma^2}} e^{-\frac{(y_i^{(j)} - I_p)}{2\sigma^2}} \tag{3.2}$$

   where $j = 1, 2, ..., s$ and I_p is the peak photocurrent.

2. From each bit probabilities, the SISO RLL decoder calculates probabilities of s-bit codeword as

$$p(y_i|\bar{c}_i) = \prod_{j=1}^{s} p(y_i^{(j)}|\bar{c}_i^{(j)}) \tag{3.3}$$

   It should be noticed that there are 2^q possible codewords $\bar{c}_i$ in total.

3. Each $\bar{c}_i$ is the unique value that created by mapping rule M from the correspoding input c_i. As a result,

$$p(y_i|c_i) = p(y_i|\bar{c}_i) \tag{3.4}$$

4. The l-th bit probabilites in c_i are calculated by marginalizing the joint probability as

$$p(y_i^{(l)}|c_i^{(l)} = \epsilon) = \sum_{c_i^{(l)} = \epsilon} p(y_i|c_i) \tag{3.5}$$

where $\epsilon \in \{0, 1\}$ and $l = 1, 2, ..., q$.

5. Finally, the LLR value $z_i^{(l)}$ is produced as

$$z_i^{(l)} = \log \frac{p(y_i^{(l)}|c_i^{(l)} = 0)}{p(y_i^{(l)}|c_i^{(l)} = 1)} \tag{3.6}$$

where this LLR value is used as the input of a soft-decision FEC decoder afterwards.

3.3 Polar Codes

Polar codes, proposed by Arikan in 2009, provide a novel idea for the capacity-approaching code construction and create a new field of coding theory.
A polar code can be specified completely by $(N, K, \mathcal{I})$, where N is the length of a codeword in bits, K is the length of information bits vector u and $\mathcal{I} = |K|$ is the set of *information bit indices*. The remaining indicates subset $\mathcal{F} = |N - K|$ is called as *frozen bit indices* [41]. For a $(N, K, \mathcal{I})$ polar code, $R = K/N$ is the code rate and N is the power of 2. Let $n = \log_2(N)$ and $\mathbf{G} = \mathbf{F}^{\otimes n} = \mathbf{F} \otimes ... \otimes \mathbf{F}$(n copies) is the n-fold Kronecker product of Arikan's [42] standard polarizing kernel $\mathbf{F} = \begin{bmatrix} 1 & 1 \\ 0 & 1 \end{bmatrix}$. Then a codeword is generated as Eq. (3.7).

$$x = u.\mathbf{G}_{\mathcal{I}} = \mathbf{d}.\mathbf{F}^{\otimes n} \tag{3.7}$$

where $\mathbf{d}$ is a vector of N bits length including *information bits* and *frozen bits* such that $\mathbf{d}_{\mathcal{I}} = u$ and $\mathbf{d}_{\mathcal{F}} = 0$, respectively. Polar codes follow the form in Eq. (3.7) are non-systematic codes.

$$\begin{aligned}
x_1 &= u_1 \oplus u_2 \oplus u_3 \oplus u_4 \oplus u_5 \oplus u_6 \oplus u_7 \oplus u_8 \\
x_2 &= u_5 \oplus u_6 \oplus u_7 \oplus u_8 \\
x_3 &= u_3 \oplus u_4 \oplus u_7 \oplus u_8 \\
x_4 &= u_7 \oplus u_8 \\
x_5 &= u_2 \oplus u_4 \oplus u_6 \oplus u_8 \\
x_6 &= u_6 \oplus u_8 \\
x_7 &= u_4 \oplus u_8 \\
x_8 &= u_8
\end{aligned} \tag{3.8}$$

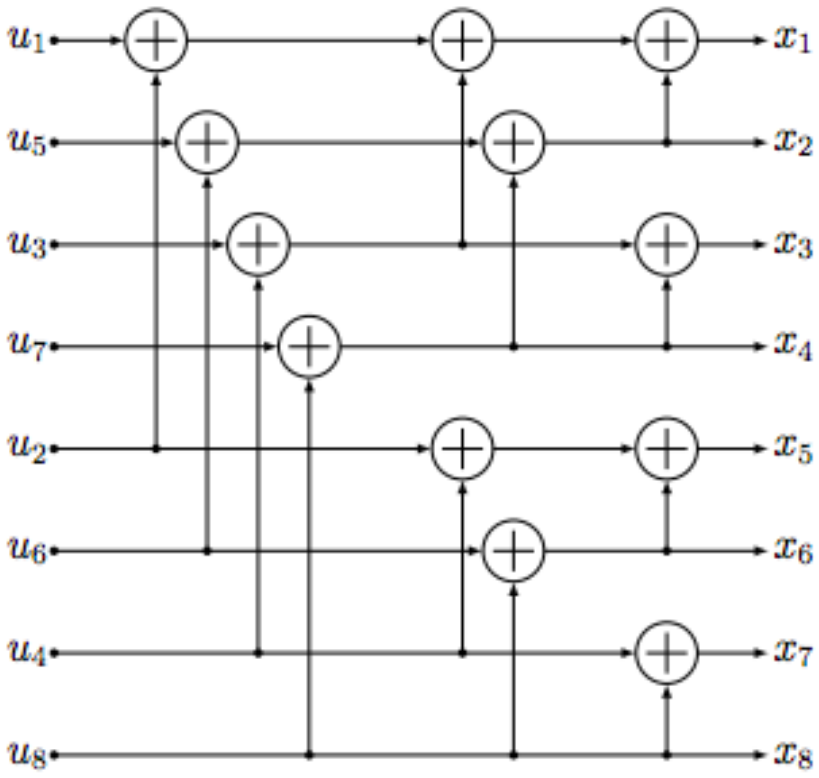

Figure 3.2. The factor graph representation of 8-bit Polar encoder, G_8.

On the other hand, a systematic polar code can be described as an equivalent to original polar code, except that the information vectors are mapped to codewords, such that the information bits are explicitly visible [41]. The most popular decoding algorithm for Polar code is the Successive Cancelation (SC) algorithm which is also introduced by Arikan.

Algorithm 1 Successive Canellation Decoding

Input: Code block length N, received codeword y^N,
information set $\mathcal{A}$, and frozen bit vector $u_{\bar{\mathcal{A}}}$.

Output: estimated information bit, $\hat{u}_{\mathcal{A}}$

for $i = N$ to 1 **do**
  if $(i \notin \mathcal{A})$ **then**
    $\hat{u_i} \leftarrow u_i$
  else
    if $\log\left(\frac{W_i(y^N, \hat{u}_{i-1}|0)}{W_i(y^N, \hat{u}_{i-1}|1)}\right) \geq 0$ **then**
      $\hat{u_i} \leftarrow 0$
    else
      $\hat{u_i} \leftarrow 1$
    end if
  end if
end for
return $\hat{u}_{\mathcal{A}}$

3.4 Simulation Results

In this section, we present simulation results for the joints of SISO 4B6B RLL code ($q = 4; s = 6$) with Polar codes. In each Polar code, both Non-systematic (Polar-Nonsys) and Systematic (Polar-Sys) are considered to make comparisons with the combination of SISO 4B6B and BLS RS codes over GF(2^4) which were investigated in [33]. Three code rates of Polar codes $(64, 44)$, $(64, 28)$, and $(64, 12)$ are used to compare with that of the reference BLS RS codes (15,11), (15,7), and (15,3), respectively.

As is highlighted in Figure 3.3, Figure 3.4, and Figure 3.5 the BER performances of proposed schemes are better than those of the reference BLS RS codes at all corresponding code rates. In the highest code rate case , the gains of proposed scheme nearly 4.5 dB (Polar-Nonsys) and 4.7 dB (Polar-Sys) than BLS RS (15,11). Furthermore, while the BER performances of BLS RS codes are reduced when the code rates decrease from the highest $(15, 11)$ to the lowest code rate $(15, 3)$, the BER performances of 4B6B-Polar codes show opposite trends.

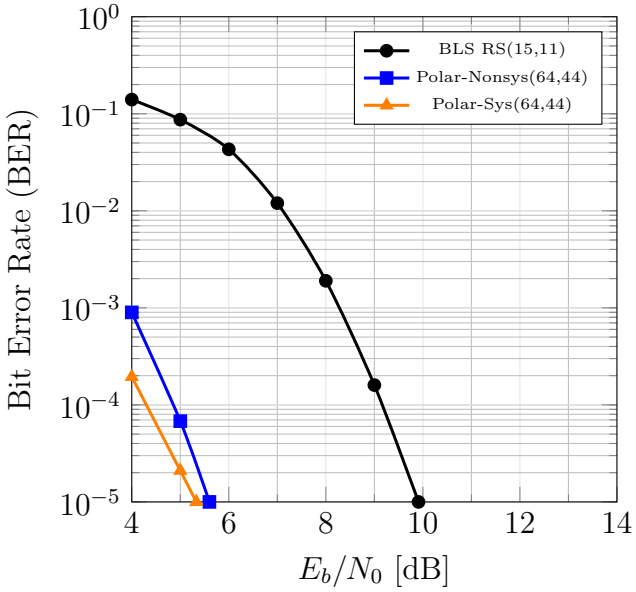

Figure 3.3. BER performances of the proposed SISO 4B6B-Polar(64,44) and BLS RS(15, 11) codes.

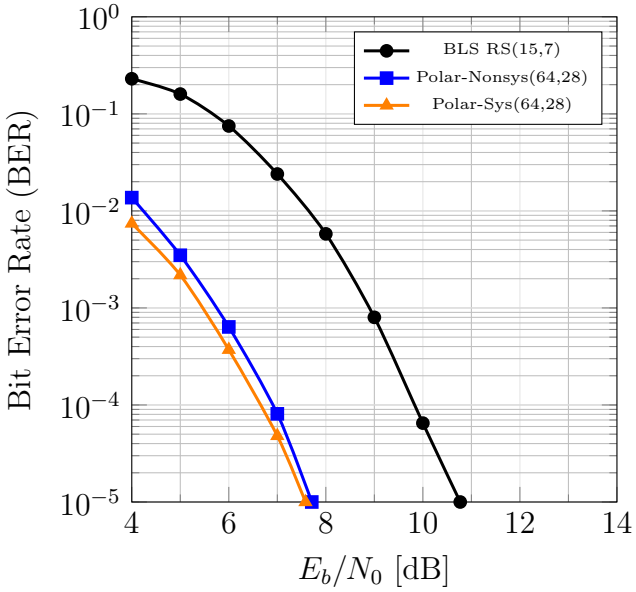

Figure 3.4. BER performances of the proposed SISO 4B6B-Polar (64, 28) and BLS RS (15, 7) codes.

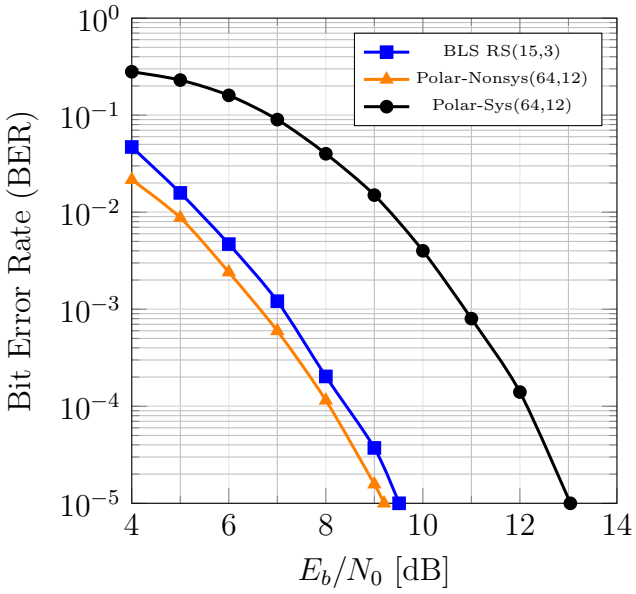

Figure 3.5. BER performances of the proposed SISO 4B6B-Polar (64, 12) and BLS RS (15,3) codes.

For the lowest code rate,the proposed scheme (Polar-Nonsys and Polar-Sys) can archive BER = 10^{-5} when E_b/N_0 are 9.60 dB and 9.20 dB while BLS RS (15,3) requires E_b/N_0 up to 13.0 dB. It is because Polar code is constructed based on channel polarization, which indicates that some sub-channels tend to be more robust and others to be weaker. Then, the robustest sub-channels is incrementally selected for information bits. Moreover, the Systematic Polar code has higher BER performance compared with Non-systematic Polar at the same code rate. We next compared the FER performances in Figure 3.6, Figure 3.7, Figure 3.8. To calculate the FERs, one codeword corresponds to one frame. It can be clearly seen that the proposed schemes outperform BLS RS codes in all cases.

3.5 Summary

In this chapter, we have presented a joint of Polar and Run-Length Limited scheme as a strong FEC candidate for VLC systems. With the proposed scheme, the number of 1's and 0's in codewords are exactly the same. Simulations proposed algorithm exhibit significantly better performance than the BLS RS codes.

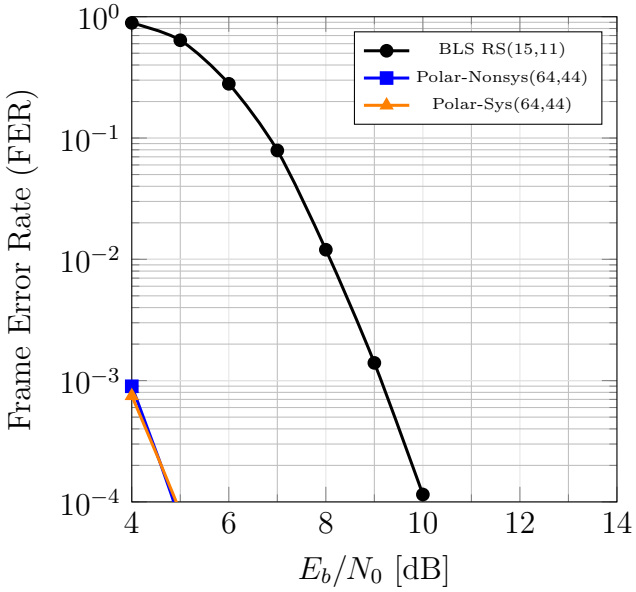

Figure 3.6. FER performances of the proposed SISO 4B6B-Polar (64, 44) and BLS RS (15, 11) codes.

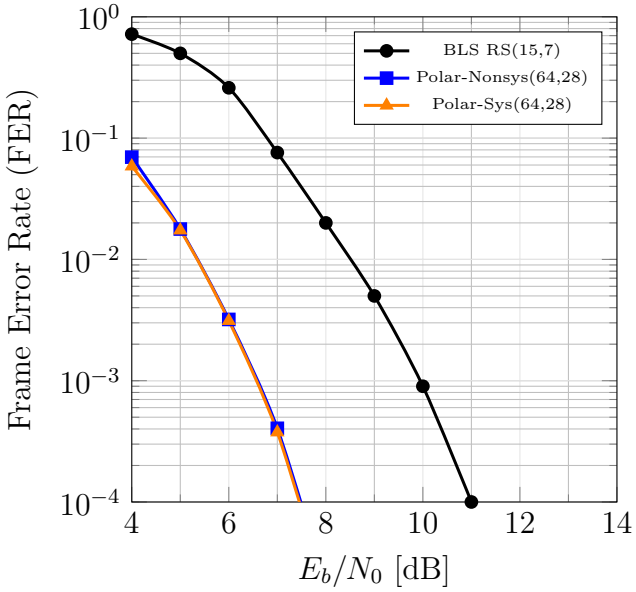

Figure 3.7. FER performances of the proposed SISO 4B6B-Polar (64, 28) and BLS RS (15, 7) codes.

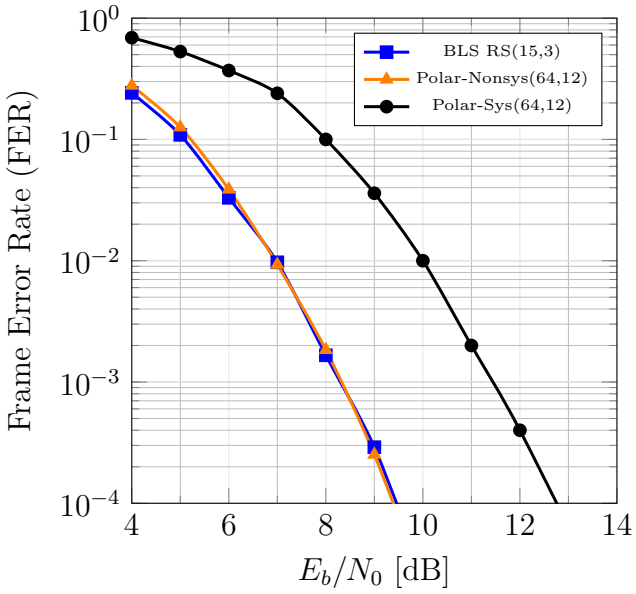

Figure 3.8. FER performances of the proposed SISO 4B6B-Polar (64, 12) and BLS RS (15, 3) codes.

An interesting future direction would be to consider practical VLC systems with hardware impelementation.

4 Log-Likelihood Ratio Calculation using Low-bit Soft-Decision for Error Correction in Visible Light Communication Systems

4.1 Introduction

In the last few years, lighting market has experienced enormous changes due to the light-emitting diodes (LEDs) revolution. The modern LEDs, which have outstanding advantages in terms of energy efficiency, long service life, and colour rendering capacity, have been replacing the use of incandescent lamps in the whole wide world [43]. This has paved a way for the rise of visible light communication (VLC) technology. In VLC systems, since the received signals are often limited by several forms of noises, Forward Error Correction (FEC) codes are essential to ensure a reliable data transmission and extend the distances. Run-length limited (RLL) codes were also widely used to support DC balance, clock recovery, and flicker mitigation. Three practical RLL codes including Manchester, 4B6B, and 8B10B were provided to co-operate with Reed-Solomon (RS) or concatenated RS and Convolutional Code (CC) FEC codes in IEEE 802.15.7 standard [29]. The lighting lams using LEDs have outstanding advantages compared with the traditional light sources. With the power of white light, LEDs can provide higher efficiency in lumen output while the power consumption is lower or the same.

RLL codes generally show no error correction ability and produce coding overheads that limit the performance of FEC codes. As a result, many researchers have considered about FEC codes that not only archive better error correction performance but also keep the DC balance in VLC systems. The third-generation FEC codes such as Turbo code and Low-density parity-check (LDPC) were investigated in [32], [33] with substantial performance improvements. Unfortunately, the power of "soft-decision" cannot be used because traditional RLL decoders or de-scramblers only work with hard-decision technique. Recently, the authors in [37] developed new soft-input soft-output (SISO) RLL decoding algorithm to concatenate with soft-decision FEC decoders. The joint of SISO RLL and various FEC decoding schemes was conceived in [44], [45]. In their research, the VLC

system was modeled as an on-off keying (OOK) modulation over a linear optical Additive White Gaussian Noise (AWGN) channel which is described as

$$y(t) = R.x(t) * h(t) + n(t) \tag{4.1}$$

where $y(t)$ represents the received signal, $x(t)$ is the transmitted signal, R is the photo dectector (PD) responsivity (A/W), $*$ denotes convolution, and $n(t)$ is Additive White Gaussian Noise (AWGN) which contains shot and thermal noises with the variance σ^2 [26].

In the case of AWGN channels, a sequence of LLRs is used to passed to the soft decoder, expressed by

$$LLR(y_i) = \ln \frac{P(x_i = 0|y_i)}{P(x_i = 1|y_i)} \tag{4.2}$$

where y_i is the received sample and the conditional probability is generally calculated as

$$P(x_i|y_i = \Delta) = \frac{1}{\sqrt{2\pi\sigma_\Delta^2}} e^{-\frac{(y_i - \mu_\Delta)^2}{2\sigma_\Delta^2}} \tag{4.3}$$

where μ_Δ and σ_Δ are the mean value and standard deviation for $\Delta = 0, 1$.

However, calculations of exact LLR follow this kind of model (*Gaussian approximation*) are quite complicated for a practical implementation.

In this study, we propose a new method which can help calculate the LLR values from the received signal of IM/DD VLC systems. It consists of two components: a 3-bit soft-decision decider and LLR transformer. The state-of-the-art Polar code [41] is used to verify the effectiveness of proposed method.

4.2 3-bit Soft-Decision Decider

An N-bit soft-decision receiver makes use of $2^N - 1$ decision thresholds to determine the *likelihood functions* of the received samples, where N is the number of quantization bits. In the case of $N = 3$, the received samples are compared with $2^3 - 1 = 7$ thresholds V_{th+3} to V_{th-3} as shown in Figure 4.1. The PD converts the received optical signal to an electrical signal that is amplified by the transimpedance amplifier (TIA). The amplified signal is fed to the 3-bit decider that consists of seven comparators ($C_{-3}, C_{-2}, C_{-1}, C_0, C_1, C_2, C_3$). The hard-decision

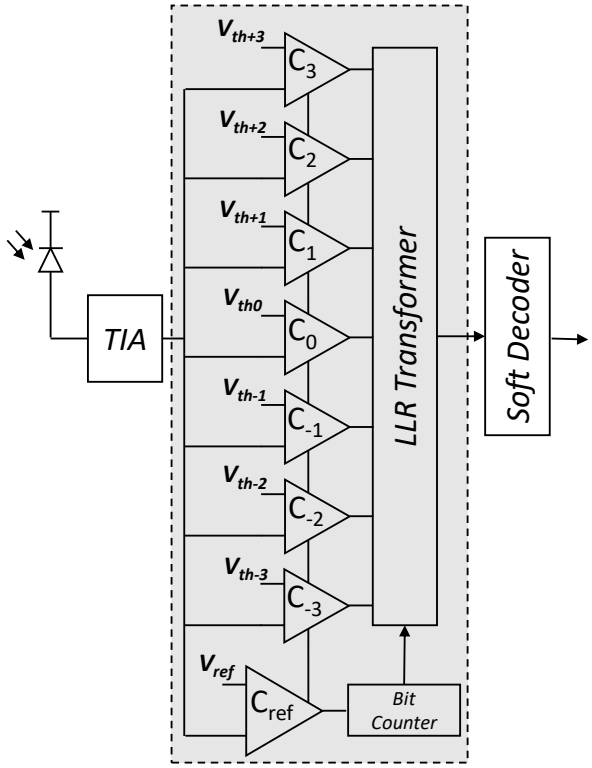

Figure 4.1. Proposed 3-bit Soft-Decision Receiver.

bit is regenerated from the central comparator C_0 while other soft-decision bits are determined from the soft-decision thresholds V_{th+3}, V_{th+2}, V_{th+1} and V_{th-1}, V_{th-2}, V_{th-3}. The seven outputs from the comparators are arranged as binary vectors from [0,0,0,0,0,0,0] to [1,1,1,1,1,1,1] and passed to LLR tranformer for LLR values generation. Finally, soft decoder makes use LLR values to decode data. The optimum threshold values can be pre-calculated by using automatic threshold tracking algorithm [46] through C_{ref} and Bit Counter blocks.

4.3 LLR Transformer

In this section, we apply the *transformation method* introduced in [47] to statistically characterize the VLC channel and use it to generate LLR values to be provided to the soft decoder. The basic idea of this method is to transform a

uniformly-distributed random variable x into a new random variable y with the probability density function (pdf) $P(y|x)$, defined as

$$y(x) = \mathbf{F}^{-1}(x) \tag{4.4}$$

where $\mathbf{F}(x)$ is the cumulative distribution function (CDF) of y.

In 3-bit soft-decision receiver, we characterize the optical channel by evaluating the CDF for eight possible decided binary vectors ([0,0,0,0,0,0,0], [0,0,0,0,0,0,1], ..., [1,1,1,1,1,1,1]). In details, we created a mapping table which gives the values of $\mathbf{F}^{-1}(x_i)$, where x_i is the i^{th} bit of a uniformly distributed random variable x and $\mathbf{F}^{-1}(x_i)$ is the CDF for the decision valuable when a bit zero or one is transmitted. From the table, we calculate $P(y_i|x_i)$ and the conditional probability $P(x_i|y_i)$ as expressed by

$$P(x_i|y_i) = \frac{P(y_i|x_i)P(x_i)}{P(y_i|x_i=0)P(x_i=0) + P(y_i|x_i=1)P(x_i=1)} \tag{4.5}$$

where $P(x_i)$ is the *a priori probability* of uniformly distributed random variable x.

Finally, the $LLR(y_i)$ is calculated by using Eq. **??**. Table 2 shows a simulation result example for the LLR calculation. Detail information is presented in the next section.

Table 2. Monte Carlo simulation result example for LLR calculation at $E_b/N_0 = 5$.

3-bit soft-decision value											
D_3	D_2	D_1	D_0	D_{-1}	D_{-2}	D_{-3}	$\mathbf{F}^{-1}(x_i=0)$	$\mathbf{F}^{-1}(x_i=1)$	$P(x_i=0\|y_i)$	$P(x_i=1\|y_i)$	$LLR(y_i)$
0	0	0	0	0	0	0	3413940	1026537	0.2845	0.0855	1.2017
0	0	0	0	0	0	1	301608	209802	0.0251	0.0175	0.3630
0	0	0	0	0	1	1	288638	231996	0.0241	0.0193	0.2185
0	0	0	0	1	1	1	272453	255155	0.0227	0.0213	0.0656
0	0	0	1	1	1	1	249254	267377	0.0208	0.0223	-0.0702
0	0	1	1	1	1	1	227900	281603	0.0190	0.0235	-0.2116
0	1	1	1	1	1	1	206350	294218	0.0172	0.0245	-0.3547
1	1	1	1	1	1	1	1039987	3433182	0.0867	0.2861	-1.1943

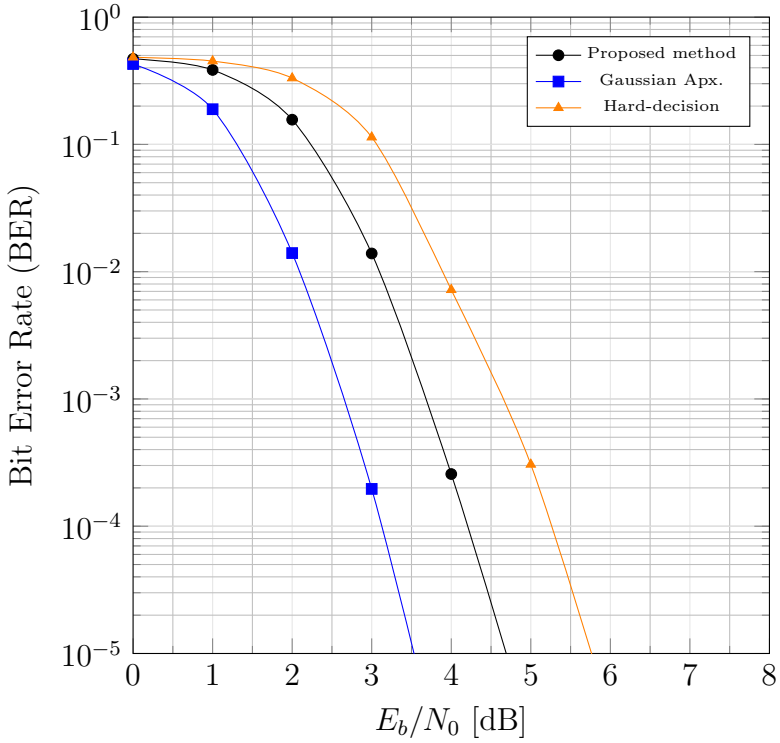

Figure 4.2. BER performances of non-systematic Polar codes (1024,512) using proposed method, Gaussian approximation and hard-decision technique.

4.4 Simulation Results

To verify the effectiveness of the proposed method, Monte Carlo simulations are used in Matlab. For VLC channel, we use the channel environment and parameters for determining noise variances in [26]. In the simulations, fixed energy per bit to noise power spectral density ratio (E_b/N_0) values from 0dB to 10dB are used or fair comparison.

Fistly, 12x10^6 uniformly-distributed random binary bits are sent from the transmitter to the receiver. At the receiver, the reference comparator (C_{ref}) will be swept from 0 to the peak voltage V_p to count the number of zero and one using Bit counter. Those thresholds at which the ratio of zero and one are approximated to 1:1, 3:1, 1:3 are set as V_{th0}, V_{th-3}, V_{th+3}; while the remaining thresholds V_{th+2}, V_{th+1}, V_{th-1}, V_{th-2} will be calculated as $2/3(V_{th+3} - V_{th+0})$, $1/3(V_{th+3} - V_{th+0})$, $2/3(V_{th0} - V_{th-3})$, $1/3(V_{th+0} - V_{th-3})$, respectively. Next, threshold values are

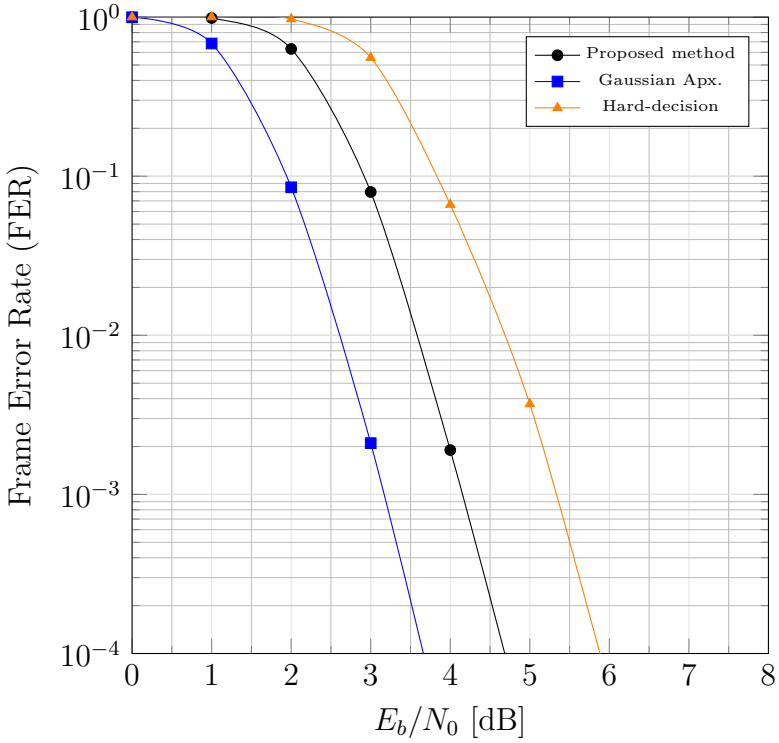

Figure 4.3. FER performances of non-systematic Polar codes (1024,512) using proposed method, Gaussian approximation and hard-decision technique.

applied to count and create a mapping table, such as Table 2.

In Table 2, the columns $\mathbf{F}^{-1}(x_i = 0)$ and $\mathbf{F}^{-1}(x_i = 1)$ represent the number of time the specific binary vector in a row is generated when transmitted data was zero or one. The conditional probabilities that a zero and one is transmitted are given in column $P(x_i = 0|y_i)$ and $P(x_i = 1|y_i)$, calculated by Eq. 4.5. The LLR value of each binary vector is then calculated using Eq. 4.2 and is given in column $LLR(y_i)$.

Finally, the error correction performance of the non-systematic Polar code (1024,512) using 3 bit soft decision technique (Proposed method) was evaluated in terms of Bit Error Rate (BER) and Frame Error Rate (FER), compared with the same Polar code using two different methods, ie., *Gaussian approximation* (Gaussian Apx.) and hard-decision technique.

As can be seen in Figure 4.2, the (E_b/N_0) gain of the proposed method is

nearly 1dB than hard-decision technique at $BER = 10^{-5}$. However, the Gaussian approximation method, which calculate the LLR value for each received data, shows the best (E_b/N_0) gain with at least 1dB than proposed method. Figure 4.3 shows the FER performances with similar (E_b/N_0) gain at $FER = 10^{-4}$.

4.5 Summary

In this chapter, we have presented an alternative method which will be provided to the soft decoder in VLC systems. The proposed method is composed of 3-bit soft-decision decider and LLR transformer. Simulation results have shown that the Polar decoder using proposed technique offers a better performance than hard-decision technique. Although the performance of our method cannot beat the Gaussian approximation approach, it provides a promising direction to apply soft-decision FEC schemes in practical VLC systems.

5 Deep Learning based RLL-FEC Decoding Scheme for Visible Light Communication Systems

5.1 Introduction

In recent years, deep learning (DL) has gained a huge attraction and shown significant success in various research areas such as speech recognition, computer vision, and so on [48]. Inspired by these achievements, researchers have applied deep learning technologies as alternative approaches to solve problems in communication systems including modulation recognition [49], and channel decoding [50], [51], [52], [53]. Furthermore, several studies proposed replacing the structure of conventional communication systems by a deep learning-based end-to-end communication system [49], [54], [55].

In this chapter, a novel low-bit analog-to-digital converters (ADCs) DL-based method which jointly decodes the concatenated FEC-RLL code in VLC systems is presented. We first proposed the use of low-bit ADCs with few-bit precision in the system to collect more information on the received samples. The number of bits representing each sample pass through the DL-based decoder afterward. Because of the success in solving sequence problems and great decoding performance [52], recurrent neural networks (RNNs) are chosen as DL architecture in this paper. The combination of SISO RLL and Polar decoding scheme [39] which showed best error-correction performance among related works is considered as the state-of-the-art decoder for comparison. The main contributions are summarized as follows:

- We originally propose a joint RLL-FEC decoding method that combines low-bit ADCs and light-weight RNN architecture in VLC system.
- We confirm that DL-based decoder can recover the original data at VLC receiver with slight error-correction performance loss and significantly improving in the computation complexity compared to the state-of-the-art decoder.
- The computation time of the proposed decoders on various hardware platforms confirms the capability of using DL-based decoders with filicker mit-

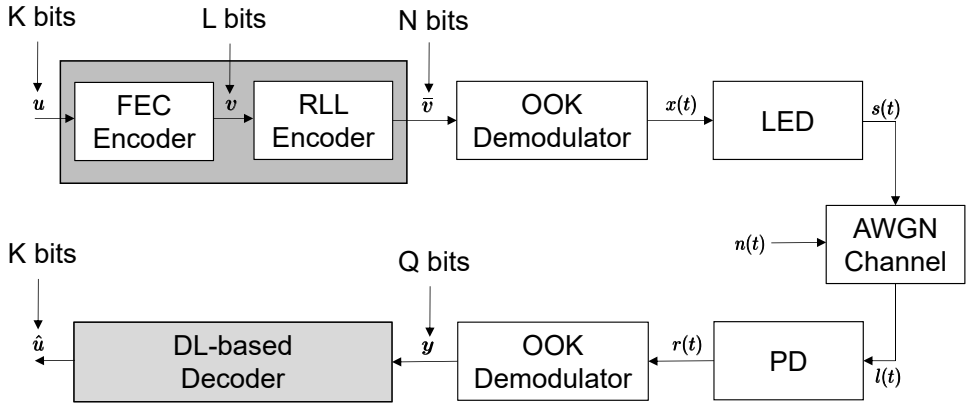

Figure 5.1. Block diagram of the proposed VLC system.

igation in VLC system.

Notation specification: Bold capital letters refer to matrices and bold lowercase letters represent vectors. Also, the subscript on a lowercase letter u_i represents the *i-th* element of vector $\boldsymbol{u}$.

5.2 System Model

Figure 5.1 depicts the general block diagram of the proposed VLC system, which relies on a concatenated FEC and RLL coding scheme at the transmitter; whereas deep learning-based decoder is used to recover the information at the receiver.

At the transmitter, the K-bit information sequences $\boldsymbol{u} \triangleq [u_0, u_1, ..., u_{K-1}]$ is firstly used by the FEC encoder to generate the L-bit codeword $\boldsymbol{v} \triangleq [v_0, v_1, ..., v_{L-1}]$. Every L-bit in the FEC-encoded codewords are mapped to N-bit codeword in $\bar{\boldsymbol{v}} \triangleq [\bar{v}_0, \bar{v}_1, ..., \bar{v}_{N-1}]$ by a RLL encoder afterwards, based on a mapping rule that guarantees the DC balance at the output. The resultant $\bar{\boldsymbol{v}}$ is converted into on-off keying (OOK) signal $\boldsymbol{x(t)}$, which is subsequently used to drive the LED front-end circuit producing $\boldsymbol{s(t)}$ signal for both lighting and data transmission.

After passing through the VLC channel, the optical signal emitted from the LED is received by the photodetector at the receiver. The received signal $\boldsymbol{r(t)}$ is given as $\boldsymbol{r(t)} = \gamma.\boldsymbol{s(t)} * \boldsymbol{l(t)} + \boldsymbol{n(t)}$, where γ is photo detector (PD) responsivity (A/W); $\boldsymbol{l(t)}$ is the impluse response of the channel; $*$ denotes convolution; and $\boldsymbol{n(t)}$ is additive white gaussian noise (AWGN) which contains shot noise, thermal

noise, and intersymbol interference (ISI) [56]. In the OOK-based VLC system, the receive signal-to-noise ratio (SNR_{rx}) is given as

$$SNR_{rx} = \frac{(\gamma.P_r)^2}{\sigma^2_{shot} + \sigma^2_{thermal} + (\gamma.P_{ISI})^2}, \tag{5.1}$$

where P_r is the average power of electrical signal $\boldsymbol{x(t)}$, P_{ISI} is the average power of intersymbol interference, σ^2_{shot} and $\sigma^2_{thermal}$ are the variances of the shot noise and thermal noise, respectively.

The OOK demodulator takes the electrical signal $\boldsymbol{r(t)}$ as input and delives as output the sequences $\boldsymbol{y}$. In the case of hard-decision technique, the *i-th* value of y_i is determined as follows:

$$y_i = \begin{cases} 1, & \text{if } r_i \geq V_{th} \\ 0, & \text{otherwise} \end{cases}, \tag{5.2}$$

where V_{th} is the hard-decision threshold voltage..

On the other hand, the OOK demodulator can compute the corresponding soft information in the form of *log-likelihood ratios* based on the *Gaussian appoximation*, given as:

$$LLR(y_i) = ln\frac{p(y_i|\bar{c}_i = 0)}{p(y_i|\bar{c}_i = 1)}, \tag{5.3}$$

where the conditional probabilities are generally calculated as:

$$p(y_i|\bar{c}_i = \Delta) = \frac{1}{\sqrt{2\pi\sigma^2_\Delta}} e^{-\frac{(y_i - \mu_\Delta)^2}{2\sigma^2_\Delta}}, \tag{5.4}$$

where μ_Δ and σ_Δ are the mean value and standard deviation for $\Delta = 0, 1$, respectively.

In the IM/DD VLC systems, the transmission is only one direction from the transmitter to the receiver in which the transmitted signal is directly proportional to the LED's intensity and is non-negative values. When the LED light strikes the photodetector, a voltage is generated in the external circuit proportional to the intensity of the incident light. Thus, calculating the LLRs based on the *Gaussian appoximation* is not feasible in the real system. In the proposed system, we propose the use of low-bit OOK demodulator to quantize the received voltage into binary sequences and pass to DL-based decoder afterwards. The configuration of low-bit OOK demodulator is presented in the next section.

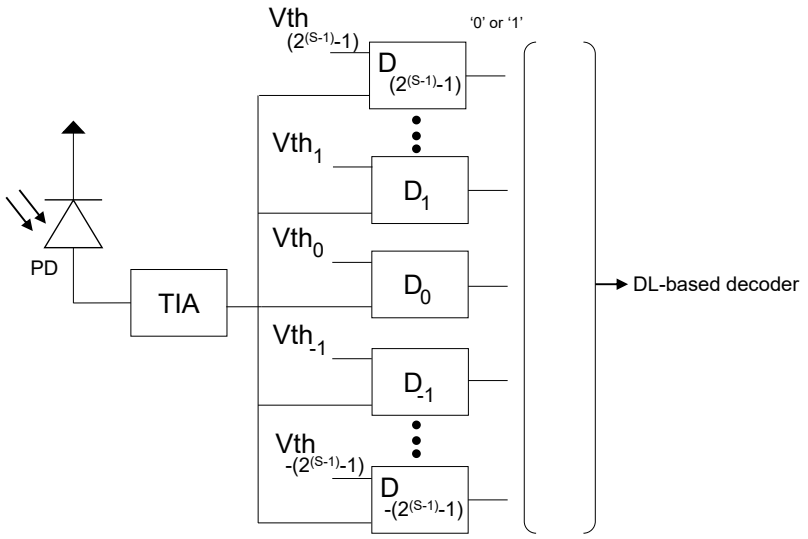

Figure 5.2. Low-bit OOK demodulator configuration in proposed VLC system.

5.3 Low-bit OOK demodulator

From the practical implementation point of view, we employ the low-bit (1-3 bits) OOK demodulator for the proposed VLC system as can be seen in Figure 5.2. In the *S-bit* OOK demodulator, where S is the number of bit precision, 2^S-1 decision thresholds are used such that the middle threshold determines the hard-decision bit, while the other thresholds identify the certain of the hard-decision bit though confident decision bits. As can be seen from the Figure 5.2, the photodetector converts the incident light to electrical signals which are consequently amplified by the trans-impedance amplifier (TIA). The amplified signal is passed to *S-bit* decider which consists of 2^S-1 comparators ($D_{-(2^{(S-1)}-1)}$, $D_{-(2^{(S-1)})}$, ...,D_{-1}, D_0, D_1, $D_{(2^{(S-1)})}$, $D_{(2^{(S-1)}-1)}$). The hard-decision bit is generated by comparing the amplified signal with the central threshold of V_{th0}. Similarly, other confident decision bits are determined from $D_{-(2^{(S-1)}-1)}$, $D_{-(2^{(S-1)})}$, ...,D_{-1} and D_1, ...,$D_{(2^{(S-1)})}$, $D_{(2^{(S-1)}-1)}$. The 2^S-1 outputs from the comparators are arranged to a binary vector and fed to the RNN-based decoder.

Finally, the RNN-based decoder makes use the provided vectors $\boldsymbol{y} \triangleq [y_0, y_1, ..., y_{Q-1}]$ to estimate information sequences $\hat{\boldsymbol{u}} \triangleq [\hat{u}_0, \hat{u}_1, ..., \hat{u}_{K-1}]$. It is noticed that, $Q = N$ when the hard-decision bits or soft LLRs values are produced in the OOK de-

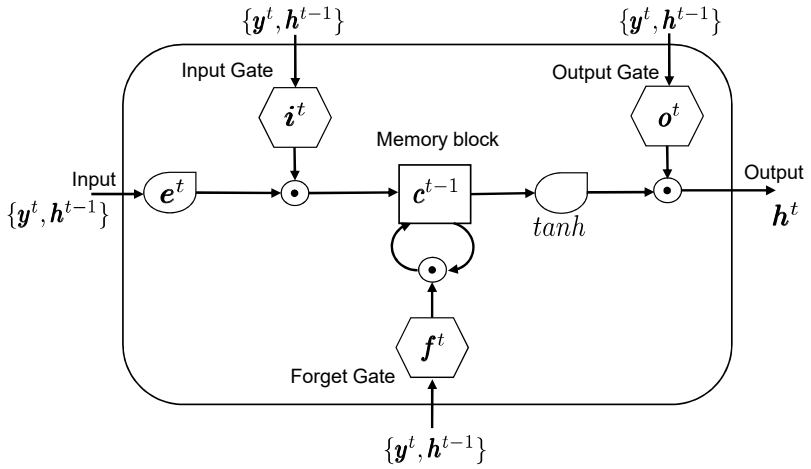

Figure 5.3. A basic LSTM cell.

modulator; $Q = (2^S - 1).N$ if the *S-bit* OOK demodulation technique is applied.

5.4 Deep Learning-based Decoder

In this section, we give a brief introduction to the concept of RNN and describe the architecture of RNN-based decoder for OOK-based VLC systems.

5.4.1 RNN preliminaries

Recurrent neural networks (RNNs) is a type of artificial neural network designed to make use of sequential information. Unlike in a traditional neural network where all inputs and outputs are considered to be independent, a typical RNN with feedback loops (recurrent edges) and the output at current time step depends on the current input as well as previous stage via recurrent edges. Training an RNN is handled by a backpropagation algorithm called *backpropagation through time (BPTT)*. Since RNNs trained with BPTT have difficulties in capturing long-term dependencies due to vanishing/exploding gradient problem, Long Short-Term Memory network (LSTMs), a special type of RNNs that can learn long-term dependencies, is widely adopted in practice. In this paper, we use LSTM to propose the RNN-based decoder and the terms RNN/LSTM can be used interchangeably with the same meaning.

A typical LSTM network comprises different memory blocks called LTSM cells. In each LSTM cell, the prevous cell state $\boldsymbol{c}^{t-1}$ and hidden state $\boldsymbol{h}^{t-1}$ are used with the input to produce the current cell state $\boldsymbol{c}^t$ and hidden state $\boldsymbol{h}^t$ that are being tranferred to the next LSTM cell. The hidden state and cell state have same vector size defined by number of nodes in cell. Let denote M as number of nodes, then we have $\boldsymbol{c}^t, \boldsymbol{h}^t \in \mathbb{R}^{M\times 1}$. As can be seen from Figure 5.3, a memory block is responsible for adding or removing information to the cell state and it is done through structures called gates. A gate includes a sigmoid neural net layer followed by a pointwise multiplication operator and controlled by a concatenation of the output (or hidden state) $\boldsymbol{h}^{t-1}$ from previous time step and the current input $\boldsymbol{y}^t \in \mathbb{R}^{Z\times 1}$. An LTSM contains three gates including forget gate which decides what information to be removed from the cell state, input gate which controls what new information is added to the cell state from the current input, and output gate which decides which is going to output from the cell state. The equations to compute the values of three gates are described as follows:

$$\boldsymbol{i}^t = \sigma(\boldsymbol{W}^{yi}\boldsymbol{y}^t + \boldsymbol{W}^{hi}\boldsymbol{h}^{t-1} + \boldsymbol{b}^i), \tag{5.5}$$

$$\boldsymbol{f}^t = \sigma(\boldsymbol{W}^{yf}\boldsymbol{y}^t + \boldsymbol{W}^{hf}\boldsymbol{h}^{t-1} + \boldsymbol{b}^f), \tag{5.6}$$

$$\boldsymbol{o}^t = \sigma(\boldsymbol{W}^{yo}\boldsymbol{y}^t + \boldsymbol{W}^{ho}\boldsymbol{h}^{t-1} + \boldsymbol{b}^o), \tag{5.7}$$

$$\boldsymbol{e}^t = \tanh(\boldsymbol{W}^{ye}\boldsymbol{y}^t + \boldsymbol{W}^{he}\boldsymbol{h}^{t-1} + \boldsymbol{b}^e), \tag{5.8}$$

where σ is the elementwise logistic sigmoid activation function and *tanh* is elementwise hyperbolic tangent activation function. $\boldsymbol{i}$, $\boldsymbol{f}$, and $\boldsymbol{o} \in \mathbb{R}^{M\times 1}$ are the input gate, forget gate, and output gate, respectively. In addition, $\boldsymbol{W}^{yi}$, $\boldsymbol{W}^{yf}$, $\boldsymbol{W}^{yo}$, $\boldsymbol{W}^{yc} \in \mathbb{R}^{M\times Z}$, $\boldsymbol{W}^{hi}$, $\boldsymbol{W}^{hf}$, $\boldsymbol{W}^{ho}$, $\boldsymbol{W}^{hc} \in \mathbb{R}^{M\times M}$, $\boldsymbol{b}^i$, $\boldsymbol{b}^f$, $\boldsymbol{b}^o$, $\boldsymbol{b}^e \in \mathbb{R}^{M\times 1}$ are the variable weights and bias to be computed during the training process. Finally, cell state $\boldsymbol{c}^t$ and hidden state $\boldsymbol{h}^t$ are given by (5.9) and (5.10) respectively:

$$\boldsymbol{c}^t = \boldsymbol{f}^t \odot \boldsymbol{c}^{t-1} + \boldsymbol{i}^t \odot \boldsymbol{e}^t, \tag{5.9}$$

$$\boldsymbol{h}^t = \boldsymbol{o}^t \odot \tanh(\boldsymbol{c}^t), \tag{5.10}$$

where $\odot$ denotes element-wise multiplication of two vectors (Hadamard product).

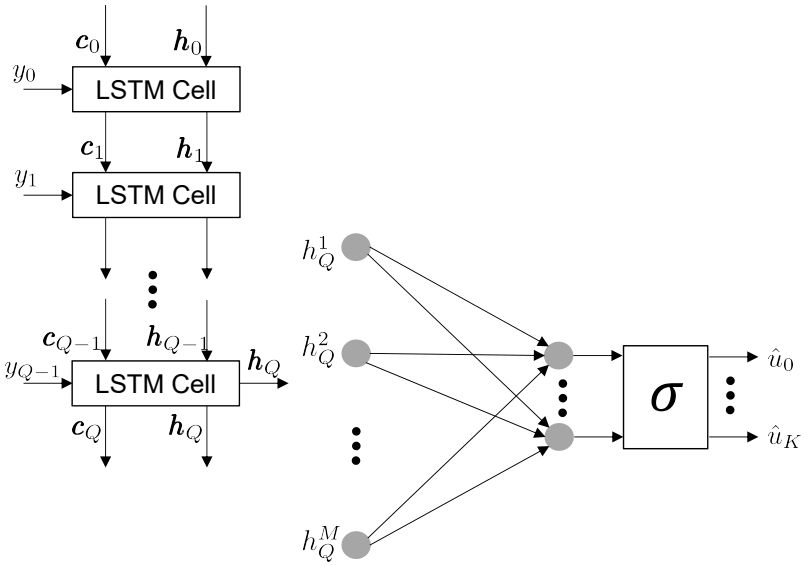

Figure 5.4. Proposed RNN architecture.

5.4.2 Proposed RNN-based Decoder

The proposed LSTM structure for the joint RLL and FEC decoder in VLC system takes a Q-dimensional output from OOK demodulator data $\boldsymbol{y} \in \mathbb{R}^{1\times Q}$ as an input data and outputs K-dimensional estimated $\hat{\boldsymbol{u}} \in \mathbb{R}^{1\times K}$. The LSTM architecture includes one LSTM layer, followed by a fully-connected layer as can be seen in Figure 5.4. The LSTM layer contains a chain of Q repeated LSTM cells which have the same structure. The current input of LSTM is $y^t \in \boldsymbol{y} \triangleq [y_0, y_1, ..., y_t, ..., y_{Q-1}]$, while the outputs $\boldsymbol{h^t}$ and $\boldsymbol{c^t}$ are Mx1 vectors, and only one LTSM cell operates in each time step.

The last fully-connected layer with M inputs $\boldsymbol{h}^Q$ and K outputs $\hat{\boldsymbol{u}}$ performs the mapping $\mathbf{f} : \mathbb{R}^{M\times 1} \rightarrow \mathbb{R}^{K\times 1}$. Since the output of DL-based decoder represents the information bits, a sigmoid function forces the output neurons to be values in the zero-to-one range, which can be inferred that the estimated bits was "1" or "0".

5.5 Training Strategy

The goal of the learning process is to find optimal parameters (weights and bias) in which the difference between the actual output of DL-based decoder $\hat{\boldsymbol{u}}$ and the target transmission bit (or label) $\boldsymbol{u}$ is minimized. This depends mainly on the choice of loss function for training. In this work, the mean squared error (MSE) is chosen as the loss function, which is defined as:

$$L_{MSE} = \frac{\|\boldsymbol{u} - \hat{\boldsymbol{u}}\|^2}{K}, \tag{5.11}$$

The goal of the learning process is to find optimal parameters (weights and bias) in which the difference between the actual output of DL-based decoder $\hat{\boldsymbol{u}}$ and the target transmission bit (or label) $\boldsymbol{u}$ is minimized. This depends mainly on the choice of loss function for training. In this work, the mean squared error (MSE) is chosen as the loss function, which is defined as:

$$L_{MSE} = \frac{\|\boldsymbol{u} - \hat{\boldsymbol{u}}\|^2}{K}, \tag{5.12}$$

To train the network, we prepared the dataset which includes both transmitted information sequence $\boldsymbol{u}$ and corresponding received vector $\boldsymbol{y}$. In VLC systems, the general sample can be generated by randomly pick the information sequences $\boldsymbol{u}$ and pass it through the channel encoder, RLL encoder, OOK modulator, and AWGN channel to obtain the received vector $\boldsymbol{y}$ as described in Fig. 5.1. For the simulation results in Section 5.6, hard-decision (or 1-bit) sequences calculated by Eq. (5.2) are firstly considered as the received vector $\boldsymbol{y}$ to train and test the DL-based decoder. Besides, we created the dataset using 2-bit and 3-bit OOK demodulator as shown in Fig. 5.2.

In both 2-bit and 3-bit demodulators, fixed threshold values are used for the deciders. For 2-bit demodulator, there are $2^2 - 1 = 3$ comparators with the hard-decision threshold voltage is $V_{th0} = V_p/2$ and the other threshold voltages are $V_{th+1} = (V_p - V_{th0})/2$ and $V_{th-1} = V_{th0}/2$. Similarly, totally $2^3 - 1 = 7$ comparators are deployed in 3-bit deciders. The upper threholds voltages are given as $V_{th+3} = 3/4(V_p - V_{th0})$, $V_{th+2} = 1/2(V_p - V_{th0})$, $V_{th+1} = 1/4(V_p - V_{th0})$, while the lower threshold voltages are calculated as $V_{th-1} = 3/4V_{th0}$, $V_{th-2} = 1/2V_{th0}$, $V_{th-3} = 1/4V_{th0}$, respectively.

5.6 Simulation Results

In this section, we provide numerical results to evaluate the performance of the DL-based decoder in the proposed VLC systems. We applied rate 1/2 Polar code for FEC code and Manchester RLL code throughout all experiments. The output dimension of an LSTM cell in Fig. 5.3 is set to 256. For the training step, a mini-batch stochastic gradient descent (SGD) method called Adam algorithm is employed with learning rate $\eta = 0.001$ and the mini-batch size is 128. The weight matrices and bias vectors of the DL-based decoder are initialized using the Xavier initialization method. Moreover, the dropout technique with probability 0.2 is used to avoid overfitting problem.

We use the channel environment and parameters in [56] for generating data. We generate 10^6 training samples to train the DL-based decoder and another 10^4 testing samples to evaluate the average SER of the trained decoder. Notably, the additive noise for training and testing steps are generated with different random seeds. We implement the simulation platform using Python 3.6 with Tensorflow 1.8.0. Table 3 summarizes the basic settings of our experiments. In all experiments, the combination of SISO Manchester and 1/2 Polar decoders (Ref. Man-Polar [39]) is used to compare with our proposed DL-based decoders.

Table 3. Basic experiment setting

Channel	AWGN
Modulation	OOK
LSTM cell size	256
Mini-batch size	128
SNR range	{-2, 0, 2, 4 ,6 , 8 ,10, 12} dB
Training samples per SNR	10^6
Testing samples per SNR	10^4
Dropout probability	0.2
Initialization method	Xavier initialization
Optimization method	Mini-batch SGD with Adam

5.6.1 Error Control Performance

In the first experiment, various configurations of the DL-based decoder are tested with the length of the information sequence $K = 4, N = 16$. The SER results for each configuration is shown in Fig 5.5. It can be observed that 1-bit demodulation DL-based decoder (1bit-RNN) with the input size $Q = 16$ shows the worst performance in all configurations. On the other hand, 3-bit demodulation DL-based decoder (3bit-RNN) with the input size $Q = (2^3 - 1).16 = 112$ almost reachs the decoding and brings up more than 1.5dB gains over the 1bit-RNN at the SER of 10^{-5}. The SER performance of 2-bit demodulation DL-based decoder (2bit-RNN) that makes use the input vectors with the size of $Q = (2^2 - 1).16 = 48$ is only 0.4 dB inferior to that of the 3bit-RNN.

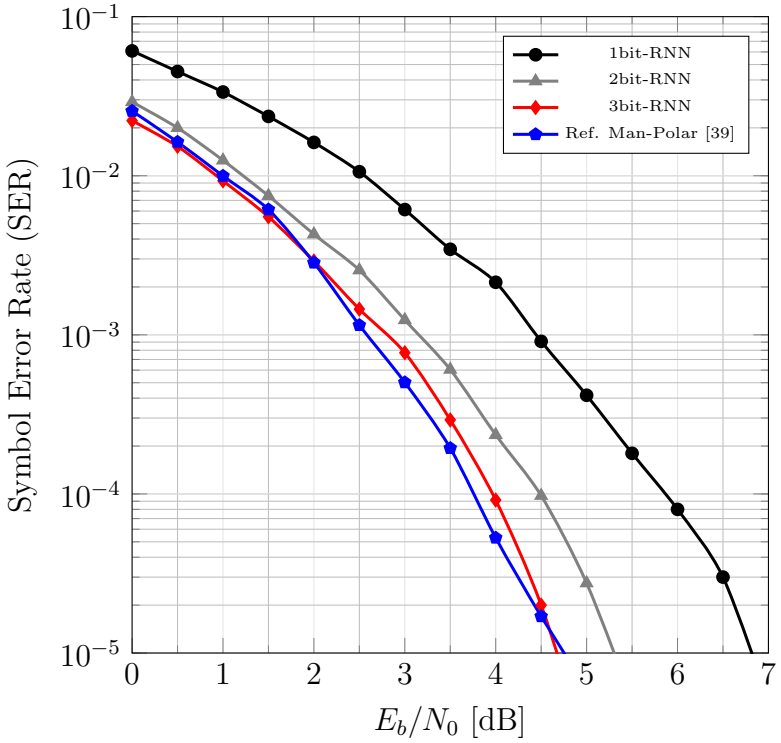

Figure 5.5. SER performance of $K = 4$, $N = 16$.

In Figure 5.6, we compare the SER performance of proposed decoders for the case $K = 8, N = 32$. We observe that the performance is getting worse compared with the case of $K = 4, N = 16$. Especially, the 3bit-RNN exhibits a remarkable

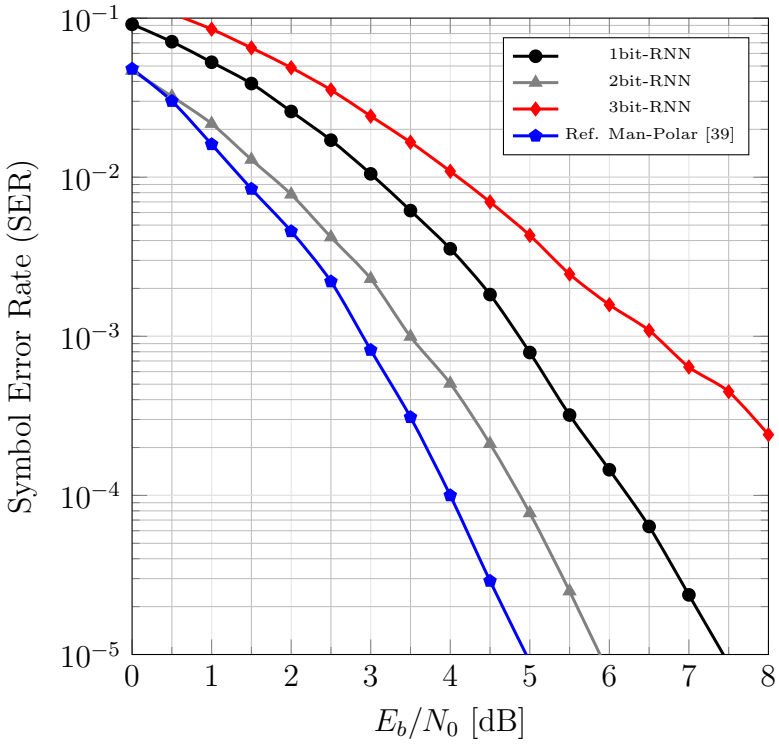

Figure 5.6. SER performance of $K = 8$, $N = 32$.

deterioration about 0.8dB gain performance gap, in comparison with the 1bit-RNN decoder at SER $= 10^{-3}$. Moreover, the SER performance of 3bit-RNN decoder is getting saturate at 5.10^{-3} in high SNR regime. It is because the size of 3bit-RNN's input vector is $(2^3 - 1).32 = 224$ which makes the relationship between the input and output of RNN too complicated to be well-learned. The phenomenon can be explained as the underfitting of the deep neural network.

5.6.2 Computation Time of Proposed Decoders

Inn order to estimate the computation time of 1bit-RNN, 2bit-RNN, and 3bit-RNN as well as the ability to apply in practice, we deploy these configurations on 3 different platforms including Intel (R) Corel (TM) i7-3970X @ 3.90GHz CPU and an NVIDIA GeForce GTX 1080 GPU (PC), NVIDIA Jetson TX2 (Jetson TX2), and Raspberry Pi 3 Model B (Raspberry Pi 3). In Fig 5.7, we provide the average time for training a mini-batch in the case of $K = 4, N = 16$. We can observe

that the proposed RNN decoders can be trained in all selected platforms. As can be seen from the figure, the training times of 1bit-RNN is approximately two times and four times faster than 2bit-RNN and 3bit-RNN, respectively. Moreover, Raspberry Pi, which has the 1.2Ghz ARMv8 Cortex-A CPU, is much slower than Jetson TX2 and PC which have dedicated GPU. Particularly, Raspberry Pi takes 6.3s for training one mini-batch, while that of Jetson TX2 and PC are 0.157s and 0.041s, respectively.

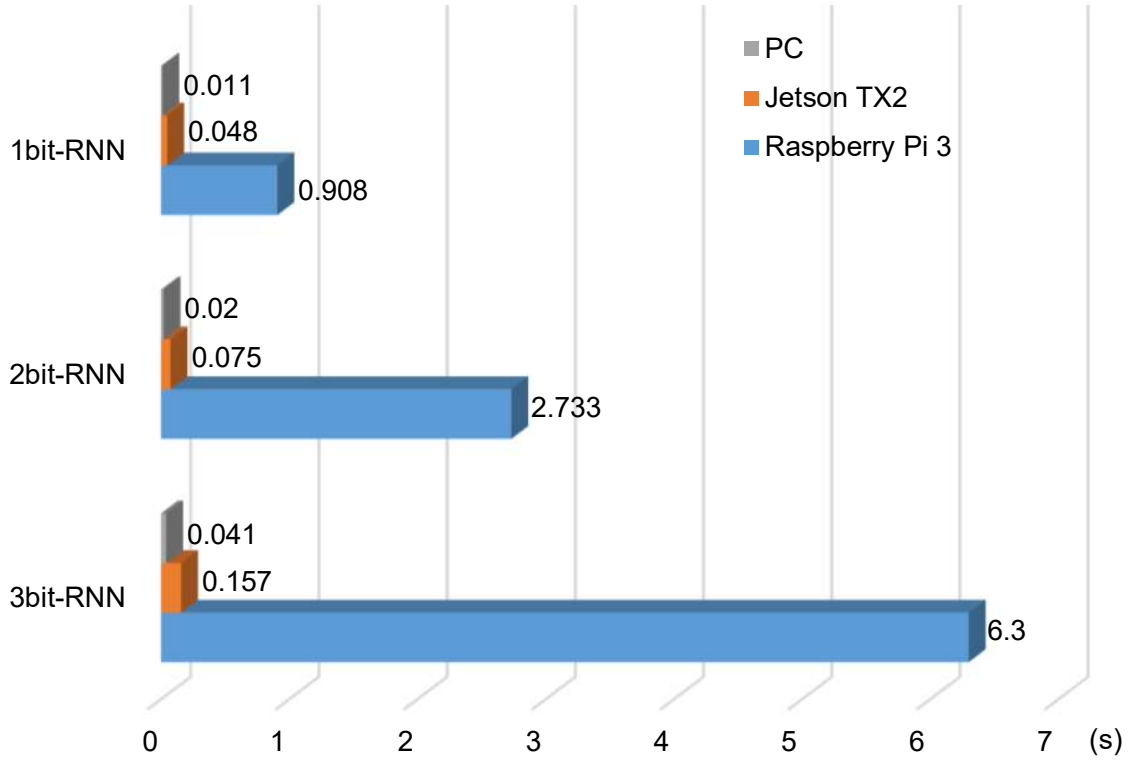

Figure 5.7. Computation time of the traning process.

Similarly, Figure 5.8 shows the average computational time for 10000 testing samples ($K = 4, N = 16$). In this experiment, we save the trained models in PC and restore in Jetson TX and Raspberry Pi 3 to make sure all platforms use the same parameters. On average, 1bit-RNN can recover 40000 information bits in 0.045s or the bandwidth B is approximately 900 kb/s; whereas, 2bit-RNN and 3bit-RNN consume about 0.136s ($B \approx 290$ kb/s) and 0.316s ($B \approx 125$ kb/s) respectively on PC. Additionally, decoding processes on Jetson TX2 are generally

Table 4. Approximate optical clock of our VLC systems on various platforms.

	1bit-RNN	2bit-RNN	3bit-RNN
PC	3.5 MHz	1.2 MHz	500 kHz
Jetson TX2	305 kHz	110 kHz	47 kHz
Raspberry Pi 3	8 kHz	2.6 kHz	1.1 kHz

ten times slower than on PC as can be seen from the figure. The computational times become much higher when Raspberry Pi 3 is used, which are about 20.2s ($B \approx 1.98$ kb/s), 61.4s ($B \approx 650$ b/s), and 142.9s ($B \approx 280$ b/s) corresponding to 1bit-RNN, 2bit-RNN, and 3bit-RNN, respectively. While the entire code rate is $R = 1/4$ for all proposed decoders, the approximate optical clock rates of the OOK-based VLC systems using three platforms are calculated as B/R and shown in Table 4.

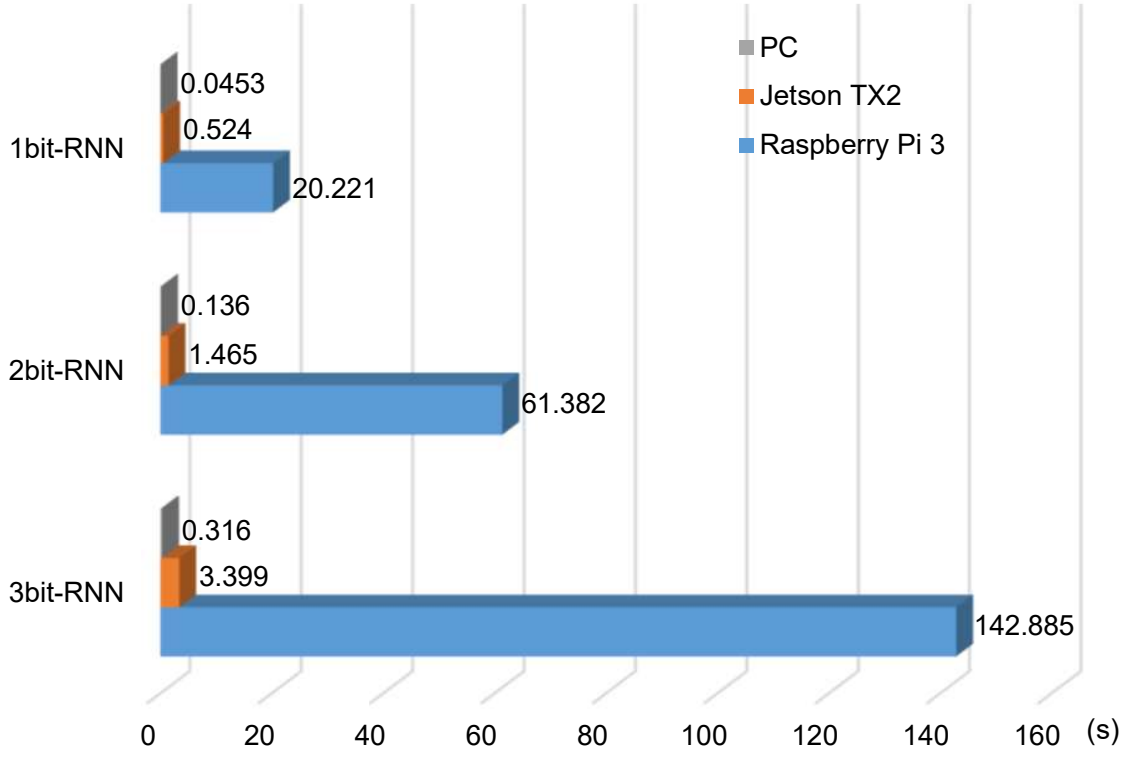

Figure 5.8. Computation time of the testing process.

As we can see from Table 4, all the optical clock rates are higher than 200 Hz

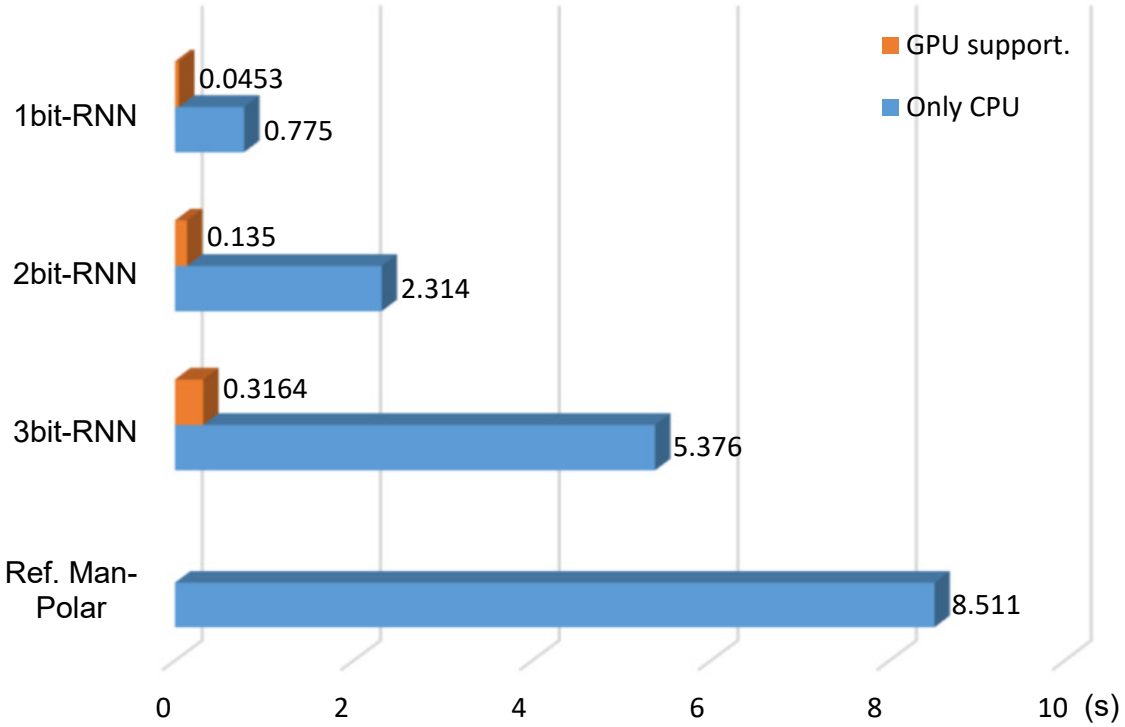

Figure 5.9. Computation time of DL-based decodes versus the state-of-the-art decoder.

(maximum flickering time period MFTP < 5 ms) which are considered safe for human eyes. It means that proposed RNN decoders can be applied in practical OOK-based VLC system even the data rate is limited when low-cost embedded platforms are used.

The DL-based decoders exhibit some performance loss compared with the Ref. Man-Polar [39] decoder, but they have superiority on the computation time (or computational complexity). Figure 5.8 shows the average computation time to decode 10000 testing samples ($K = 4$) of the DL-based decoders and the Ref. Man-Polar [39] decoder in the PC. In the case of only CPU, the 3bit-RNN, 2bit-RNN, and 1bit-RNN decoders reduce the computation time by 38%, 73%, and 91% compared to the Ref. Man-Polar [39] decoder, respectively. Also, the GPU's support can further improve the computational efficiency of DL-based decoders.

5.7 Summary

In this work, we have proposed an RNN-based RLL-FEC decoding scheme for OOK-based VLC systems. Three RNN-based architectures (1bit-RNN, 2bit-RNN, and 3bit-RNN) were comprehensively investigated in three different platforms. Numerical results indicated that proposed structures could learn efficient decoding functions with the SER performance are close to the powerful concatenating SISO RLL and Polar decoding method with the short information messages while greatly reduce the computational complexity. The results also clarify the feasibility of using deep neural networks-based decoding scheme in practical VLC receivers.

6 Conclusion

It cannot be denied that LED technology have become an essential part of our lives. LEDs devices are used for not only illumination but also automotive, advertisement, display... On the other hand, the demand for wireless transmission capacity is increasing to support the evolution of IoT systems and human requirements. In this disertation, the researcher considered an implementation of wireless data transmission using LEDs, so called VLC. In these VLC systems, RLL code is offered to mitigate flicker which is the main effect to lighting purpose. Moreover, FEC scheme is employed to enhance the transmisision reliablity.

The first contribution in Chapter 3 is about increasing the error-correction performance or transmission reliability. In this chapter, we implement concatenated Polar-RLL code to propduce flicker free codewords to be transmit in VLC system. The researcher proposes the use of soft-input soft-output RLL decoding in serial concattenation with successive cancellation Polar decoding to recover the input information. With the combination RLL and Polar codes, the BER performance will be less error compared to conventional works.

In order to have better transimission reliability, the SISO RLL decoder continuously update *a posteriori* probabilities of received signal using Gaussian approximation approach. The Gaussian approximation approach, which requires accurate knowledge of the VLC channel, is difficult to implement in practical VLC system. In Chapter 4, the dissertation presented a novel method to indrectly calculate soft information from received signal. Instead of using Gaussian approximation approach, the researcher quantilizes the received signal with a low-bit ADCs and statically characterizes the VLC channel to generate the approximate soft information.

The third contribution of this dissertation is presented in Chapter 5, which included the design of DL-based RLL-FEC decoding schemes for VLC systems. First, three RNN-based architectures was proposed. The error-correction performance of these architectures in the case of short information block length was confirmed close to the concatenation of SISO RLL-Polar decoding using using Gaussian approximation approach. Additionally, the dissertation presented that the use of DL-based decoders can greatly reduce the computational complexity.

The reseacher also clarify the feasibility of using DL-based decoding scheme in practical VLC receivers.

6.1 Future Work

The results obtained using concatenated SISO RLL and FEC decoding schemes in this dissertation highlighted the importance of its soft information calculation to obtain a better improvement in the BER. The first future work is related to the design of OOK demodulator in VLC system. Previously, we considered the use of low-bit ADC to ditermine the confidence bits of the received signal. However, it is also possible to use ADCs with different quantilize levels. Depending on channel conditions, it is also possible to use ADC with high quantilize levels; although, the incease in the ADCs' cost and the impact in the final performance has to be taken into consideration.

Since current results in this dissertation is collected from simulation, another important future work is the hardware implementation of the SISO RLL-FEC decoders. The VLC's receiver has to be designed and impelementd in the field-programmable gate arrays (FPGAs) in order to experimentally investigate different parameters such as BER, power consumption, and hardware resource.

Finally, our future work for the contribution in Chapter 5 includes possible improvements in the following aspects:

- ***LSTM structure and optimization:*** In the current implementation, we have just employed RNN architectures with the original setting for LSTM cell, optimization method, and lost function. To find a stable, high-performance RNN structure, other LTSM architecture and its hyperparameter should be investigated.

- ***Information block lengths:*** As can be seen from Section 5.6, the current RNN-based decoders show great error-correction performance at short information block $K = 4$ or $K = 8$ and its performance decrease when block lengths increase. To overcome this challenge, new architectures or incorporated structures should be further investigated.

- ***Unstable channel condition:*** In this work, the channel condition between transmitter and receiver is stable for messages transmission. How-

ever, channel parameters could be varied during one symbol period in actual systems; such channel condition should be taken into consideration in future research.

References

[1] G. Abadal, J. Alda, and J. Agustí. Electromagnetic Radiation Energy Harvesting–The Rectenna based Approach. In *ICT-Energy-Concepts Towards Zero-Power Information and Communication Technology*. IntechOpen, 2014.

[2] M. Akanegawa, Y. Tanaka, and M. Nakagawa. Basic Study on Traffic Information System using LED Traffic Lights. *IEEE Transactions on Intelligent Transportation Systems*, 2(4):197–203, 2001.

[3] Cisco Visual Networking Index: Forecast and Trends, 2017–2022. `https://www.cisco.com/c/en/us/solutions/collateral/service-provider/visual-networking-index-vni/white-paper-c11-741490.html`. Accessed: 2019-05-10.

[4] Q. M. Qadir, T. A. Rashid, N. K. Al-Salihi, B. Ismael, A. A. Kist, and Z. Zhang. Low Power Wide Area Networks: A Survey of Enabling Technologies, Applications and Interoperability Needs. *IEEE Access*, 6:77454–77473, 2018.

[5] X. Wang, L. Kong, F. Kong, F. Qiu, M. Xia, S. Arnon, and G. Chen. Millimeter wave communication: A comprehensive survey. *IEEE Communications Surveys Tutorials*, 20(3):1616–1653, thirdquarter 2018.

[6] Global Lighting Accociation. Strategic Roadmap of the Global Lighting Industry. `http://www.globallightingassociation.org/`. Accessed: 2019-05-10.

[7] Japan Lighting Manufacturers Association. Lighting Vision 2030. `https://www.jlma.or.jp/`. Published: 2019-03-05.

[8] S. H. Lee, S. Jung, and J. K. Kwon. Modulation and Coding for Dimmable Visible Light Communication. *IEEE Communications Magazine*, 53(2):136–143, Feb 2015.

[9] S. Rajagopal, R. D. Roberts, and S. Lim. IEEE 802.15.7 Visible Light Communication: Modulation Schemes and Dimming Support. *IEEE Communications Magazine*, 50(3):72–82, March 2012.

[10] S. M. Berman, D. S. Greenhouse, I. L. Bailey, R. D. Clear, and T. W. Raasch. Human Electroretinogram Responses to Video Displays, Fluorescent Lighting, and Other High Frequency Sources. *Optometry and Vision Science: official publication of the American Academy of Optometry*, 68(8):645–662, 1991.

[11] Y. Tanaka, T. Komine, S. Haruyama, and M. Nakagawa. Indoor visible light data transmission system utilizing white led lights. *IEICE Trans. Commun., B*, 86(8):2440–2454, aug 2003.

[12] H. Haas et al. Wireless Data from Every Light Bulb. *TED Global. Edinburgh, Scotland*, 20, 2011.

[13] H. Haas. LiFi is A Paradigm-Shifting 5G Technology. *Reviews in Physics*, 3:26 – 31, 2018.

[14] M. Y. Abualhoul, O. Shagdar, and F. Nashashibi. Visible Light Inter-vehicle Communication for Platooning of Autonomous Vehicles. In *2016 IEEE Intelligent Vehicles Symposium (IV)*, pages 508–513. IEEE, 2016.

[15] L. Cheng, W. Viriyasitavat, M. Boban, and H. Tsai. Comparison of Radio Frequency and Visible Light Propagation Channels for Vehicular Communications. *IEEE Access*, 6:2634–2644, 2018.

[16] H. Lv, L. Feng, A. Yang, P. Guo, H. Huang, and S. Chen. High Accuracy VLC Indoor Positioning System with Differential Detection. *IEEE Photonics Journal*, 9(3):1–13, 2017.

[17] P. Du, S. Zhang, C. Chen, A. Alphones, and W. D. Zhong. Demonstration of A Low-Complexity Indoor Visible Light Positioning System using An Enhanced TDOA Scheme. *IEEE Photonics Journal*, 10(4):1–10, 2018.

[18] N. Q. Pham, V. P. Rachim, and W. Y. Chung. High-Accuracy VLC-based Indoor Positioning System Using Multi-Level Modulation. *Opt. Express*, 27(5):7568–7584, Mar 2019.

[19] M. Kim and T. Suh. A Low-Cost Surveillance and Information System for Museum Using Visible Light Communication. *IEEE Sensors Journal*, 19(4):1533–1541, 2018.

[20] P. Ji, H. Tsai, C. Wang, and F. Liu. Vehicular Visible Light Communications with LED Taillight and Rolling Shutter Camera. In *2014 IEEE 79th Vehicular Technology Conference (VTC Spring)*, pages 1–6, May 2014.

[21] I. Takai, T. Harada, M. Andoh, K. Yasutomi, K. Kagawa, and S. Kawahito. Optical Vehicle-to-Vehicle Communication System Using LED Transmitter and Camera Receiver. *IEEE Photonics Journal*, 6(5):1–14, Oct 2014.

[22] A. Duque, R. Stanica, H. Rivano, and A. Desportes. Off-the-Shelf Bi-Directional Visible Light Communication Module for IoT Devices and Smartphones. In *EWSN 2017-13th International Conference on Embedded Wireless Systems and Networks*, pages 238–239. ACM, 2017.

[23] F. Miramirkhani and M. Uysal. Visible Light Communication Channel Modeling for Underwater Environments with Blocking and Shadowing. *IEEE Access*, 6:1082–1090, 2017.

[24] H. Kaushal and G. Kaddoum. Underwater Optical Wireless Communication. *IEEE Access*, 4:1518–1547, 2016.

[25] X. Li, R. Mardling, and J. Armstrong. Channel Capacity of IM/DD Optical Communication Systems and of ACO-OFDM. In *2007 IEEE International Conference on Communications*, pages 2128–2133. IEEE, 2007.

[26] T. Komine and M. Nakagawa. Fundamental Analysis for Visible–Light Communication System Using LED Lights. *IEEE Transactions on Consumer Electronics*, 50(1):100–107, 2004.

[27] J. M. Kahn and J. R. Barry. Wireless Infrared Communications. *Proceedings of the IEEE*, 85(2):265–298, 1997.

[28] Y. Qiu, H. H. Chen, and W. X. Meng. Channel Modeling for Visible Light Communications – A Survey. *Wireless Communications and Mobile Computing*, 16(14):2016–2034, 2016.

[29] IEEE Standard for Local and Metropolitan Area Networks–Part 15.7: Short-Range Wireless Optical Communication Using Visible Light. *IEEE Std 802.15.7-2011*, pages 1–309, Sept 2011.

[30] S. Kim and S. Y. Jung. Novel FEC Coding Scheme for Dimmable Visible Light Communication based on The Modified Reed–Muller Codes. *IEEE Photonics Technology Letters*, 23(20):1514–1516, 2011.

[31] S. Kim and S. Y. Jung. Modified Reed–Muller Coding Scheme Made From the Bent Function for Dimmable Visible Light Communications. *IEEE Photonics Technology Letters*, 25(1):11–13, Jan 2013.

[32] S. H. Lee and J. K. Kwon. Turbo Code-based Error Correction Scheme for Dimmable Visible Light Communication Systems. *IEEE Photonics Technology Letters*, 24(17):1463–1465, 2012.

[33] S. Kim. Adaptive FEC Codes Suitable for Variable Dimming Values in Visible Light Communication. *IEEE Photonics Technology Letters*, 27(9):967–969, May 2015.

[34] L. Feng, R. Q. Hu, J. Wang, and P. Xu. Fountain Code-based Error Control Scheme for Dimmable Visible Light Communication Systems. *Optics Communications*, 347:20–24, 2015.

[35] J. Fang, Z. Che, Z. L. Jiang, X. Yu, S. M. Yiu, K. Ren, X. Tan, and Z. Chen. An Efficient Flicker–Free FEC Coding Scheme for Dimmable Visible Light Communication Based on Polar Codes. *IEEE Photonics Journal*, 9(3):1–10, 2017.

[36] Z. Babar, M. A. M. Izhar, H. V. Nguyen, P. Botsinis, D. Alanis, D. Chandra, S. X. Ng, R. G. Maunder, and L. Hanzo. Unary-Coded Dimming Control Improves ON–OFF Keying Visible Light Communication. *IEEE Transactions on Communications*, 66(1):255–264, 2018.

[37] H. Wang and S. Kim. Bit–Level Soft Run–Length Limited Decoding Algorithm for Visible Light Communication. *IEEE Photonics Technology Letters*, 28.3:237–240, 2016.

[38] H. Wang and S. Kim. Soft–Input Soft–Output Run–Length Limited Decoding for Visible Light Communication. *IEEE Photonics Technology Letters*, 28.3:225–228, 2016.

[39] H. Wang and S. Kim. Dimming Control Systems with Polar Codes in Visible Light Communication. *IEEE Photonics Technology Letters*, 29.19:1651–1654, 2017.

[40] D. D. Le, D. P. Nguyen, T. H. Tran, and Y. Nakashima. Log-Likelihood Ratio Calculation Using 3-Bit Soft-Decision for Error Correction in Visible Light Communication Systems. *IEICE Transactions on Fundamentals of Electronics, Communications and Computer Sciences*, 101(12):2210–2212, 2018.

[41] E. Arikan. Systematic Polar Coding. *IEEE Communications Letters*, 15(8):860–862, 2011.

[42] E. Arikan. Channel polarization: A method for constructing capacity-achieving codes for symmetric binary-input memoryless channels. *IEEE Transactions on Information Theory*, 55(7):3051–3073, July 2009.

[43] A. Jovicic, J. Li, and T. Richardson. Visible Light Communication: Opportunities, Challenges and The Path to Market. *IEEE Communications Magazine*, 51(12):26–32, December 2013.

[44] Z. Babar, H. V. Nguyen, P. Botsinis, D. Alanis, D. Chandra, S. X. Ng, and L. Hanzo. Unity-Rate Codes Maximize the Normalized Throughput of ON–OFF Keying Visible Light Communication. *IEEE Photonics Technology Letters*, 29(3):291–294, 2017.

[45] D. D. Le, D. P. Nguyen, T. H. Tran, and Y. Nakashima. Joint Polar and Run–Length Limited Decoding Scheme for Visible Light Communication Systems. *IEICE Communications Express*, 7(1):19–24, 2018.

[46] H. Tagami, T. Kobayashi, Y. Miyata, K. Ouchi, K. Sawada, K. Kubo, K. Kuno, H. Yoshida, K. Shimizu, T. Mizuochi, and K. Motoshima. A 3-bit Soft-Decision IC for Powerful Forward Error Correction in 10-Gb/s Optical Communication Systems. *IEEE Journal of Solid-State Circuits*, 40(8):1695–1705, Aug 2005.

[47] G. Bosco, G. Montorsi, and S. Benedetto. Soft Decoding in Optical Systems. *IEEE Transactions on Communications*, 51(8):1258–1265, Aug 2003.

[48] Y. LeCun, Y. Bengio, and G. Hinton. Deep Learning. *Nature*, 521(7553):436, 2015.

[49] T. O'Shea and J. Hoydis. An Introduction to Deep Learning for The Physical Layer. *IEEE Transactions on Cognitive Communications and Networking*, 3(4):563–575, 2017.

[50] T. Gruber, S. Cammerer, J. Hoydis, and S. T. Brink. On Deep Learning-based Channel Decoding. In *Information Sciences and Systems (CISS), 2017 51st Annual Conference on*, pages 1–6. IEEE, 2017.

[51] E. Nachmani, E. Marciano, L. Lugosch, W. J. Gross, D. Burshtein, and Y. Be'ery. Deep Learning Methods for Improved Decoding of Linear Codes. *IEEE Journal of Selected Topics in Signal Processing*, 12(1):119–131, 2018.

[52] W. Lyu, Z. Zhang, C. Jiao, K. Qin, and H. Zhang. Performance Evaluation of Channel Decoding with Deep Neural Networks. In *2018 IEEE International Conference on Communications (ICC)*, pages 1–6. IEEE, 2018.

[53] F. Liang, C. Shen, and F. Wu. An Iterative BP-CNN Architecture for Channel Decoding. *IEEE Journal of Selected Topics in Signal Processing*, 12(1):144–159, 2018.

[54] S. Dörner, S. Cammerer, J. Hoydis, and S. T. Brink. Deep Learning Based Communication Over the Air. *IEEE Journal of Selected Topics in Signal Processing*, 12(1):132–143, Feb 2018.

[55] H. Lee, I. Lee, T. Q. S. Quek, and S. H. Lee. Binary Signaling Design for Visible Light Communication: A Deep Learning Framework. *Opt. Express*, 26(14):18131–18142, Jul 2018.

[56] T. Komine and M. Nakagawa. Fundamental Analysis for Visible–Light Communication System Using LED Lights. *IEEE Transactions on Consumer Electronics*, 50(1):100–107, Feb 2004.

Acknowledgements

First of formost, I would like to express my deep gratitude to my supervisor Professor Yasuhiko Nakashima for his valuable guidance, comments, and support for my research, Doctoral course, and this dissertation.

I would like to thank Associate Professor Takashi Nakada, Affiliate Professor Mutsumi Kimura, Assistant Professor Tran Thi Hong, and Assistant Professor Renyuan Zhang for the guidance, support, and comments they gave me and helped to improve my research.

I extend my thanks to the Ministry of Education, Culture, Sports, Science and Technology in Japan (MEXT) for the scholarship grant and financial support of my Doctoral Course in Japan.

My acknowledgement to the past and present members of the Computing Architecture Laboratory for their help and time that we spent together. To my friend in Japan and Vietnam for enjoynable moments. Also I would like to thank the international community in NAIST for the help and support during my stay here in NAIST.

Last, but not least, my profound gratitude to my family, especially my wife, Tran Duc Nam Phuong, and my lovely daughter, Le Tran Thuy Lam, for their moral supports and encouragement in every step of my life.